Hindawi
Journal of Advanced Transportation
Volume 2022, Article ID 5680599, 27 pages
https://doi.org/10.1155/2022/5680599

Research Article

Heavy-Duty Vehicle Braking Stability Control and HIL Verification for Improving Traffic Safety

Fahui Wang,[1] Yongjie Lu ,[1,2] and Haoyu Li[2]

[1]*Shijiazhuang Tiedao University, Shijiazhuang 050043, China*
[2]*State Key Laboratory of Mechanical Behavior in Traffic Engineering Structure and System Safety, Shijiazhuang 050043, China*

Correspondence should be addressed to Yongjie Lu; luyongjie@stdu.edu.cn

Received 26 March 2022; Revised 24 April 2022; Accepted 29 April 2022; Published 13 July 2022

Academic Editor: Yang Yang

The braking failure of heavy vehicles under long downhill or curved conditions may cause traffic crash and reduce road traffic efficiency. Therefore, to improve the traffic safety and braking stability of vehicles under special road conditions, a braking dynamic model and control system based on the interval uncertainty analysis are proposed, and the safety of the active control model is verified by experiments (HIL). Firstly, the interval uncertain dynamic model is established based on the Monte Carlo method, and the braking failure simulation analysis of the right front wheel of heavy vehicles is carried out in the set of three uncertain intervals. Secondly, the fuzzy PID and sliding mode controller based on yaw and centroid error are designed to find the optimal control strategy from the two kinds of control strategies for HIL experiments. Finally, the actual control effect and feasibility of these control algorithms for heavy vehicle braking under special road conditions are verified by HIL experiments. The experimental results show that under the action of the fuzzy PID control strategy, the running stability of the vehicle is significantly improved compared with no control, which effectively reduces the risk of vehicle braking failure and improves the active safety and stability of the vehicle.

1. Introduction

In recent years, with the rapid growth of heavy transport vehicles in China's highway network, traffic safety problems and complex transportation systems have gradually increased, and the reduction in traffic efficiency will also cause great economic losses [1, 2]. In the traditional traffic problems, the number of road traffic accidents caused by heavy vehicles is high, and the traffic accidents caused by braking system faults account for 45% of vehicle safety accidents [3, 4]. In 2018, in the survey of 20000 heavy vehicle accidents, about 1000 accidents occurred in the downhill stage [5, 6], and the curve traffic accidents also tended to increase. Compared with the two-axle vehicles, the three-axle heavy vehicles may have rear-end danger due to the increase in braking distance because of their large mass and inertia when braking [7]. The research on the braking stability of four-wheeled vehicles on the road is mostly based on the braking recovery of commercial vehicles, and there are few incomplete braking problems such as thermal recession or insufficient braking [8]. First of all, for most vehicles under four-wheel drive braking, the engine is front-mounted, and the front wheel bears a larger load, so the braking force distributed by the front wheel is larger than that of the rear wheel. Generally, the front-to-rear braking force ratio is 6: 4. Secondly, in heavy vehicles, the vehicle weight is mainly supported by the middle and rear axles, and the front wheel is steering wheel [9], so the front wheel distribution braking force is small, and the middle and rear wheel distribution braking force is large. Large trucks in Volvo, Scania, and Mercedes-Benz are generally equipped with front wheel brakes, and most Chinese brands have no front wheel brake distribution.

At present, in the study of braking stability of heavy vehicles, Moreno et al. [10] studied the operational stability of heavy vehicles through the relationship between suspension and tire, which is mainly divided into the following cases. In the research on active safety control of vehicles, it is

based on the lane change and obstacle avoidance of heavy vehicles, and Yakub and Mori [11] used yaw moment control and active rear steering control to optimize the stability. Yao [12] took the thermal recession research and empirical model of drum brake as the study direction, which established the corresponding finite element model, and carried out statics with modal analysis on the model, but it lacked the analysis of brake under wear condition. In the research of vehicle road conditions and road adhesion coefficient, Jiang et al. [13, 14] designed a safety speed control system for heavy vehicles on long steep slopes and curve sections and introduced a line control braking system to reduce the delay of the traditional friction braking system. Although the TruckSim simulation test includes the road slope and the effective radius of the tire as the estimated state, it has some influence on the slip and stability of the vehicle. In the research of adaptive stability control for vehicles, Li et al. [15, 16] have designed a controller-based adaptive braking torque control method and a hierarchical braking force control method. The hierarchical braking controller is proposed according to the wheel slip rate and vehicle speed condition, and the initial value of the estimated tire-road friction is readjusted to improve vehicle stability.

In addition, there are few studies on uncertain braking analysis of heavy vehicles in China and abroad, and most of them focus on brake wear and empirical model. In the analysis of non-probabilistic research using interval uncertainty, Xia et al. [17–19] introduced interval uncertain parameters to further consider the reliability analysis method of interval non-probabilistic and probabilistic mixed model. At the same time, in view of the lack of sample information on uncertain parameters of automobile disc brake system, a stability analysis method of uncertain automobile disc brake system based on interval model and fuzzy model was proposed. However, in complex engineering problems, it is usually difficult to obtain sufficient experimental data to construct the probability model. Lü H and Yu [20] used the Monte Carlo method to extract multiple traffic flow variables from the dimension of dynamic characteristics to verify the accuracy of active safety control and the incidence of traffic accidents on highways. Kang et al. [21] proposed a non-probabilistic reliability index method for safety quantification based on the description of multi-ellipsoid convex model with uncertain grouping but bounded parameters. Therefore, it can be used to further optimize the vehicle stability in incomplete braking.

The research on vehicle control strategy is mainly divided into three aspects. One is the fuzzy PID control strategy designed by fuzzy adjustment of yaw moment or braking moment, and Hui-min Li et al. [22] used the yaw rate control method to improve vehicle stability, but mainly for low-speed vehicles and high adhesion coefficient road. Li et al. [23] and others introduced the gradient control method to realize the fuzzy adjustment of braking torque, and it includes gradual deceleration and emergency parking, but did not consider the uncertainty of special road conditions. Secondly, Sun et al. [24] combine fuzzy PID control with neural network control to modify and adjust the running state of the system online. Although the fuzzy control effect is improved, the vehicle yaw control and longitudinal control still need to be further improved. Third, in the design of sliding mode control mechanism, He et al. [25–27] designed two sliding mode controllers for wheel deceleration and slip rate, which were verified for low adhesion coefficient and high adhesion coefficient. However, the wheel deceleration system was also required to have a rapid transient response to optimize the vehicle control stability.

In the research of heavy vehicle multi-body dynamic simulation and HIL experiment, Li et al. [28, 29] used the TruckSim dynamic simulation software to establish a nonlinear model of trailer combination to study its turning braking stability and added ABS auxiliary control, which has a certain optimization effect on its nonlinear model. Li et al. [30, 31] established the body model, tire model, power system model, steering system model, and braking system model by referring to the real vehicle parameters. The simulation verification was carried out according to the vehicle handling stability test standard in China, but the real vehicle hardware experiment was not carried out. Chen et al. [32, 33] designed a new hardware platform based on HIL system and verified the effectiveness of the new HIL platform through several autonomous driving experiments. However, the road conditions designed in HIL test are less than TruckSim simulation software.

To improve the braking stability, traffic safety, and traffic efficiency of heavy vehicles under special road conditions, an interval uncertain control strategy model of active safety system based on the Monte Carlo method is designed. The contributions of this study are as follows. (1) The vehicle dynamic model is designed when the vehicle is braking to reflect the changing trend of lateral acceleration and longitudinal acceleration, which provides a basis for improving the braking stability of the vehicle. Although the designed sliding mode controller has a fast response speed and shortens the braking distance to the maximum, the yaw and tail flick generated by the vehicle are also large. (2) To further reduce the yaw motion of the vehicle during braking, a fuzzy PID control strategy system is designed, compared with the sliding mode control to effectively improve the yaw angular velocity of the vehicle. Although the braking distance of the vehicle is extended, it is still in the safe range relative to the controllers.

The structure of this study is as follows: in Section 2, the uncertain Lagrange dynamic control model of heavy vehicle interval is given, and the vehicle single-wheel braking force model is set. In Section 3, two kinds of braking control strategies and multi-body dynamic simulation data for improving vehicle handling stability are given. In Section 4, HIL experiments are carried out on heavy vehicles to further verify the different dynamic responses of the brake control model, the uncontrolled model, and the effects of the brake control model on vehicle ride comfort and handling stability. We discuss our research in Section 5, which summarizes the above contents and puts forward the future research direction.

2. Vehicle Dynamic Modelling and Analysis of Braking Characteristics

2.1. Dynamic Model of Single-Wheel Complete Braking Failure. Based on the study of braking dynamics of heavy

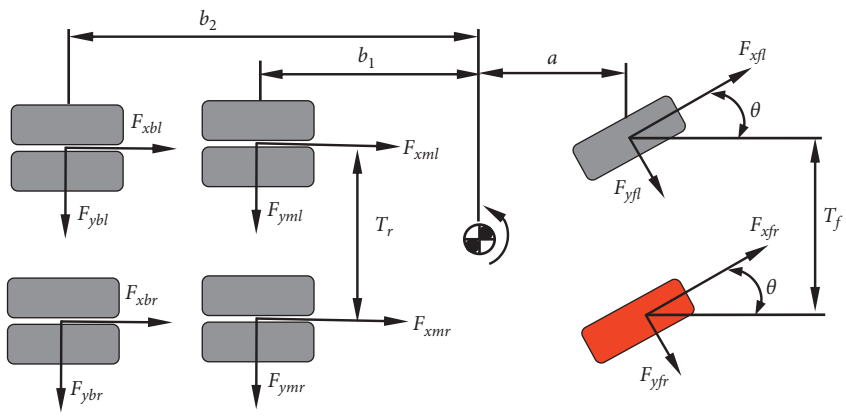

Figure 1: Vehicle dynamic model with complete brake failure (right front wheel).

three-axle vehicles, a three-degree-of-freedom model for heavy vehicles is established. Taking the right front wheel as an example in Figure 1, the vehicle dynamic model under single-wheel braking failure is established. This study assumes that the data of braking failure vehicles are consistent with those of normal vehicles, and F_{xfl}, F_{xfr}, F_{yfl}, F_{yfr}, F_{xml}, F_{xmr}, F_{yml}, F_{ymr}, F_{xbl}, F_{xbr}, F_{ybl}, and F_{ybr} are the longitudinal force and lateral force on each tire of the vehicle, respectively.

The following motion differential equation is established:

Longitudinal equation is as follows:

$$ma_x = F_{xfr}\cos\theta + F_{xfl}\cos\theta + F_{yfr}\sin\theta + F_{yfl}\sin\theta + F_{xml} + F_{xmr} + F_{xbl} + F_{xbr}. \tag{1}$$

Lateral equation is as follows:

$$ma_y = F_{xfr}\sin\theta + F_{xfl}\sin\theta - F_{yfr}\cos\theta - F_{yfl}\cos\theta - F_{yml} - F_{ymr} - F_{ybl} - F_{ybr}. \tag{2}$$

Yaw equation is as follows:

$$\begin{aligned} I_z\dot{r} = {} & \left(F_{xfr}\sin\theta + F_{xfl}\sin\theta - F_{yfr}\cos\theta - F_{yfl}\cos\theta\right)a \\ & + \left(F_{ymr} + F_{yml}\right)b_1 + \left(F_{ybr} + F_{ybl}\right)b_2 \\ & + \left(F_{xmr} - F_{xml} - F_{xbl} + F_{xbr}\right)\frac{T_r}{2} \\ & + \left(F_{xfr}\cos\theta + F_{xfl}\cos\theta + F_{yfr}\sin\theta + F_{yfl}\sin\theta\right)\frac{T_f}{2}. \end{aligned} \tag{3}$$

$F_{xfr} = 0$ is set, and according to the D' Alembert principle, the following dynamic equations are obtained. The braking failure of the right front wheel of the vehicle is marked by the red square virtual line in Figure 1.

The longitudinal balance equation is shown as follows:

$$ma_x = F_{xfl}\cos\theta + F_{yfr}\sin\theta + F_{yfl}\sin\theta + F_{xml} + F_{xmr} + F_{xbl} + F_{xbr}. \tag{4}$$

Lateral equation is as follows:

$$ma_y = F_{xfl}\sin\theta - F_{yfr}\cos\theta - F_{yfl}\cos\theta - F_{yml} - F_{ymr} - F_{ybl} - F_{ybr}. \tag{5}$$

Yaw equation is as follows:

$$\begin{aligned} I_z\dot{r} = {} & \left(F_{xfl}\sin\theta - F_{yfr}\cos\theta - F_{yfl}\cos\theta\right)a \\ & + \left(F_{ymr} + F_{yml}\right)b_1 + \left(F_{ybr} + F_{ybl}\right)b_2 \\ & + \left(F_{xmr} - F_{xml} - F_{xbl} + F_{xbr}\right)\frac{T_r}{2} \\ & \cdot \left(F_{xfl}\cos\theta + F_{yfr}\sin\theta + F_{yfl}\sin\theta\right)\frac{T_f}{2}, \end{aligned} \tag{6}$$

where m is the body mass; a is the centroid distance of the front axis; b_1 is the centroid distance of the central axis; b_2 is the centroid distance of the rear axis; γ is yaw angular velocity; θ is the front wheel angle; T_f is the front wheelbase; T_r is the middle and rear wheelbase; and F_{xfl}, F_{xfr}, F_{yfl}, F_{yfr}, F_{xml}, F_{xmr}, F_{yml}, F_{ymr}, F_{xbl}, F_{xbr}, F_{ybl}, and F_{ybr} are the longitudinal and lateral forces of each tire, respectively.

2.2. Analysis of Single-Wheel Braking Characteristics. When analyzing the single-wheel force of the vehicle, the tire is a rigid body in the ideal state, and the single-wheel braking force model of the vehicle is established, as shown in Figure 2.

V is the vehicle speed; ω is the wheel angular velocity of the vehicle; R is the rolling radius of the wheel; T_b is the braking torque; F_z is the vertical load of the vehicle; and F_x is ground breaking force.

Assuming that the vehicle load does not change during braking, and ignoring the influence of air resistance and rolling resistance, the vehicle dynamic equation can be obtained as follows:

$$m\left(\frac{dv}{dt}\right) = -F_x, \tag{7}$$

where m is the mass of single-wheel vehicle.

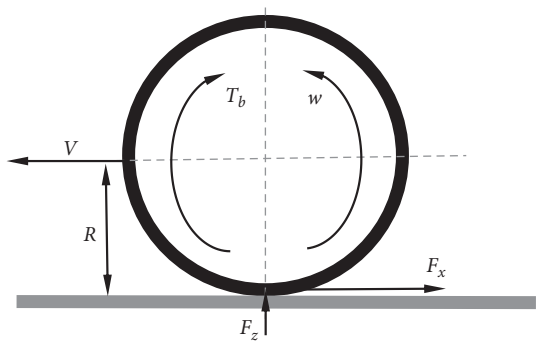

Figure 2: Single-wheel braking model.

$$J\left(\frac{dw}{dt}\right) = F_x R - T_b, \tag{8}$$

where J is the moment of inertia of the vehicle and W is the wheel angular velocity.

When the vehicle is braking, the road ignores the rolling resistance moment of the wheel, the inertia force of the vehicle at deceleration, and the inertia moment of the vehicle at turning, then the torque balance equation of any wheel with angular velocity $\omega > 0$ is as follows:

$$T_f - F_{xb} R = 0, \tag{9}$$

where T_f is the braking torque of the brake drum.

Therefore, the braking force balance equation of the brake is shown as follows:

$$\begin{cases} F_f = F_x = \dfrac{T_f}{R}, \\ F_x = \mu \cdot F_z, \end{cases} \tag{10}$$

where μ is the friction coefficient between the wheel and the ground.

When the vehicle is braking, the ground adhesion force is the maximum friction force, and the ground breaking force is the sliding friction force. The relationship between the two is shown as follows:

$$F_x < F_\varphi = \varphi_b F_z, \tag{11}$$

where F_φ is the maximum friction force between tire and ground and φ_b is the longitudinal peak adhesion coefficient.

The slip rate of wheels is defined as follows:

$$s = \frac{(v - wR)}{v}. \tag{12}$$

According to the mathematical model of tire and road surface, the relationship between road adhesion coefficient and tire slip rate can be obtained as follows:

$$\mu(s) = c_1\left(1 - e^{-c_2 s}\right) - c_3 s, \tag{13}$$

where c_1, c_2, and c_3 are the parameter values of various road surfaces, s is the slip rate of wheel and tire, and μ is the adhesion factor of road surface. The specific values of c_1, c_2, and c_3 are shown in the following Table 1.

Table 1: Tire typical road parameters and optimal slip rate.

Road	c_1	c_2	c_3	s
Ice road	0.050	306.39	0.001	0.031
Snow road	0.195	94.3	0.0646	0.06
Bitumen road (wet)	0.857	33.83	0.35	0.131
Bitumen road (dry)	1.280	23.99	0.52	0.17
Cement road (dry)	1.197	6.46	0.67	0.4

2.3. Vehicle Braking Model Based on Interval Uncertainty. If the braking system of heavy vehicles is suddenly in an unstable state in the emergency process, such as insufficient oil supply of the tubing when stepping on the brake pedal, or thermal recession when braking on a long downhill, the braking force decreases.

For the uncertain parameters of the brake and brake system changing in a certain range, whose upper and lower bounds are $\overline{x}$ and $\underline{x}$, respectively, x can be expressed as follows:

$$x = \left[\overline{x}, \underline{x}\right] \in \left\{\overline{x} \le x \le \underline{x}\right\}, \tag{14}$$

where x is called interval number or interval variable in mathematics, and it is set as the uncertain interval of braking characteristics in this section. The interval midpoint and interval radius of x can be expressed by the following equation, respectively:

$$\begin{cases} x^c = \dfrac{(\overline{x} + x)}{2}, \\ x^R = \dfrac{(\overline{x} - x)}{2}, \end{cases} \tag{15}$$

where x^c is the midpoint of the interval; x^R is the radius of the interval, which represents the dispersion of the interval values.

Interval variable x can be written in the form of midpoint radius, as shown as follows:

$$x = x^c + \delta \cdot x^R, \delta = [-1, 1], \tag{16}$$

where δ is a standardized interval variable. The uncertainty level of interval variable γ_x is defined as follows:

$$\gamma_x = \frac{x^R}{\left|x^C\right|} \times 100\%. \tag{17}$$

The uncertainty level γ_x of interval variable x is used to describe the uncertainty degree of interval variable, and its function is used to assume the change in braking failure torque parameters. If there are n interval uncertain variables, it is usually expressed by vector; i.e., $x = [x_1, x_2, x_3 \ldots x_n]^T$.

The distribution coefficient of the maximum braking torque and braking pressure of the right front wheel braking is the upper boundary, and the non-probabilistic uncertain parameter formula of γ_b is shown in the following equation:

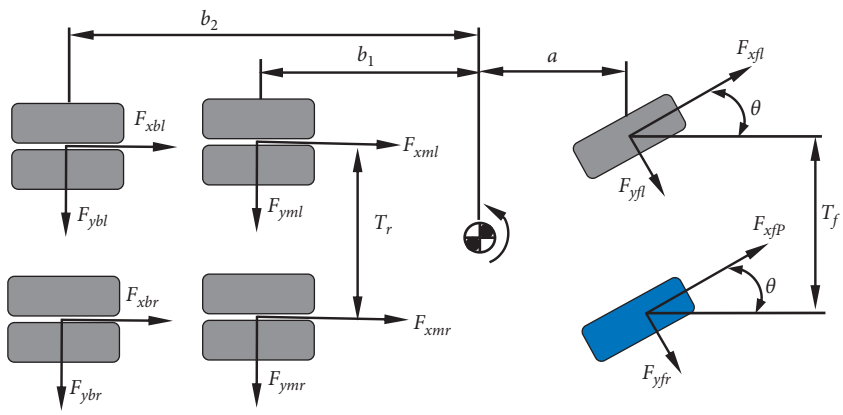

Figure 3: Dynamic model of uncertain braking failure of right front wheel.

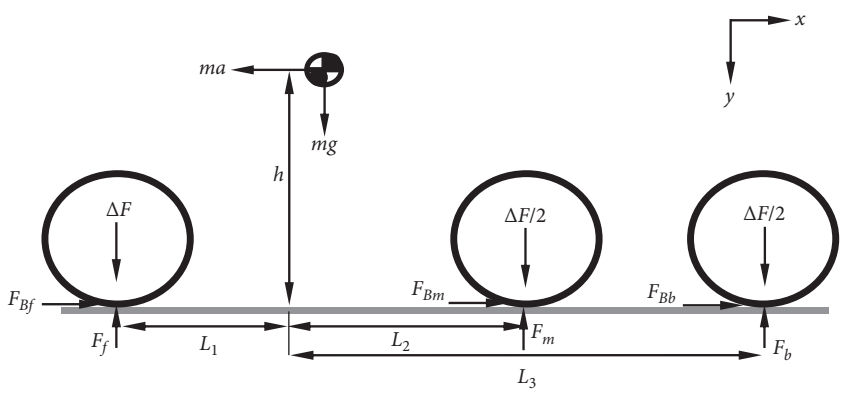

Figure 4: Right front wheel braking force distribution diagram.

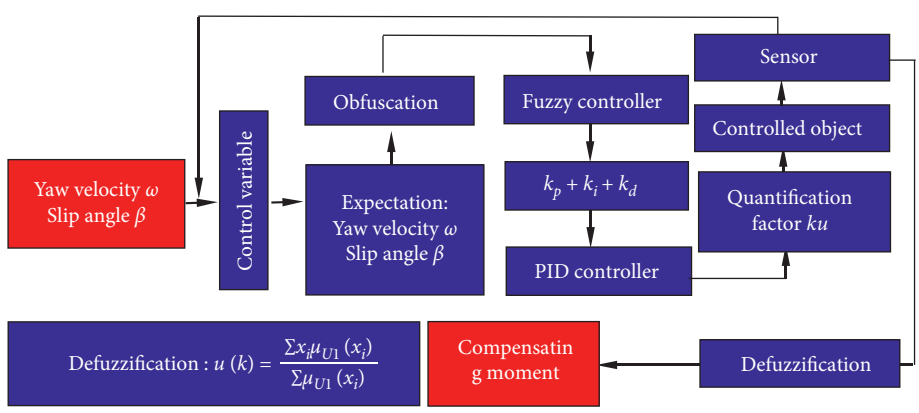

Figure 5: Schematic diagram of fuzzy PID controller.

$$\begin{cases} x = [0, 7.5] \in \{0 \le x \le 7.5\}, \\ x^c = \dfrac{(7.5 + b)}{2}, x^R = \dfrac{7.5 - b}{2}, \\ \gamma_b = \dfrac{x^R}{\left|x^C\right|} \times 100\%. \end{cases} \tag{18}$$

For the value range, the Monte Carlo method and iterative method are mostly used jointly to obtain the sampling interval value. The study in this study is for the simulation analysis of braking force. According to the actual situation and to highlight the difference in simulation data, the value basis is shown as follows:

$$\theta = \int_a^b f(x)dx, \tag{19}$$

where x_0 is randomly sampled between $[a, b]$ and x_0 is randomly sampled between $[a, b]$. The $f(x)$ value of [A, B] is replaced by $f(x_0)$, approximately $f(x) \approx b - af(x_0)$, $x_1 = 5.25$ kN, and $x_2 = 3.75$ kN.

Table 2: Fuzzy control rule table.

E U EC	NB	NM	NS	ZO	PS	PM	PB
NB	PB	PB	PB	PM	PS	ZO	NS
NM	PB	PB	PB	PM	NS	ZO	NS
NS	PB	PB	PM	PS	ZO	NS	NM
ZO	PB	PM	PS	ZO	NS	NM	NB
PS	PM	PS	ZO	NS	NM	NB	NB
PM	PS	ZO	NS	NM	NB	NB	NB
PB	ZO	NS	NM	NB	NB	NB	NB

For the value range, most of the analysis medians use the MC method and iterative method to jointly calculate the value of the sampling interval. However, this study mainly studies the braking failure, which is the simulation analysis of braking force, and does not need accuracy as a reference. According to the actual situation and to highlight the difference in simulation data, the Monte Carlo method is mainly used for the most value basis, and the iterative method can be ignored.

According to d' Alembert principle in theoretical mechanics, the motion differential equation of vehicles is as follows:

The longitudinal force balance equation of the vehicle is shown as follows:

$$ma_x = F_{xfP}\cos\theta + F_{xfl}\cos\theta + F_{yfr}\sin\theta + F_{yfl}\sin\theta + F_{xml} + F_{xmr} + F_{xbl} + F_{xbr}. \tag{20}$$

The lateral force balance equation of vehicles is shown as follows:

$$ma_y = F_{xfP}\sin\theta + F_{xfl}\sin\theta - F_{yfr}\cos\theta - F_{yfl}\cos\theta - F_{yml} - F_{ymr} - F_{ybl} - F_{ybr}. \tag{21}$$

The yaw moment balance equation of the vehicle is shown as follows:

$$\begin{aligned} I_z\dot{r} = &\left(F_{xfP}\sin\theta + F_{xfl}\sin\theta - F_{yfr}\cos\theta - F_{yfl}\cos\theta\right)a \\ &+\left(F_{ymr} + F_{yml}\right)b_1 + \left(F_{ybr} + F_{ybl}\right)b_2 \\ &+\left(F_{xmr} - F_{xml} - F_{xbl} + F_{xbr}\right)\frac{T_r}{2} \\ &+\left(F_{xfP}\cos\theta + F_{xfl}\cos\theta + F_{yfr}\sin\theta + F_{yfl}\sin\theta\right)\frac{T_f}{2}. \end{aligned} \tag{22}$$

Figure 3 shows that the uncertain failure model of the right front wheel of the vehicle is not the complete braking failure of the wheel in this attenuation process. There is a dynamic change in the attenuation process; that is, the braking effectiveness of F_{xfP} decreases from 100% to 70% and 50%. In the equation, F_{xfP} is given three or more parameter values. In this study, the braking efficiency is set to be 100%, 70%, and 50%, respectively, and it is a dynamic change value. In Figure 1, F_{xfP} is a constant value of 0.

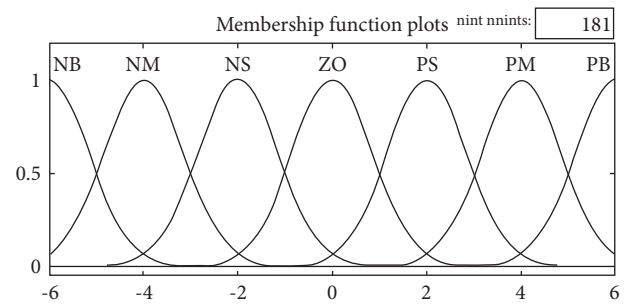

Figure 6: Input $\Delta\beta$ membership function.

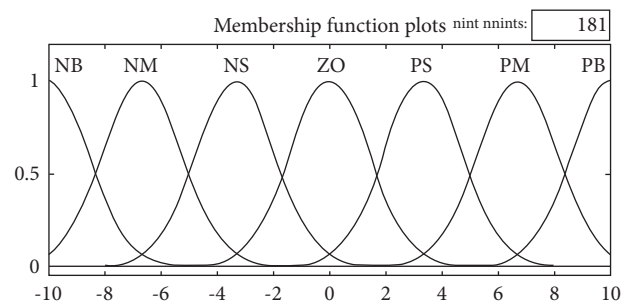

Figure 7: Input $\Delta\omega$ membership function.

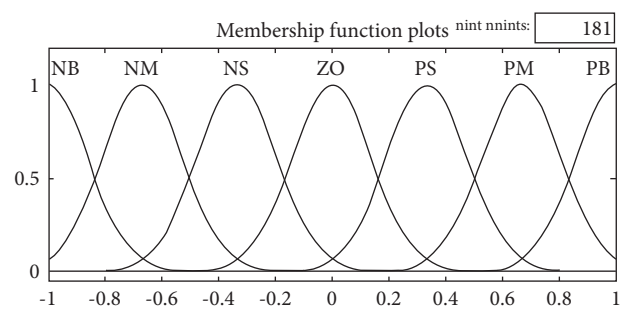

Figure 8: Output M_Z membership function.

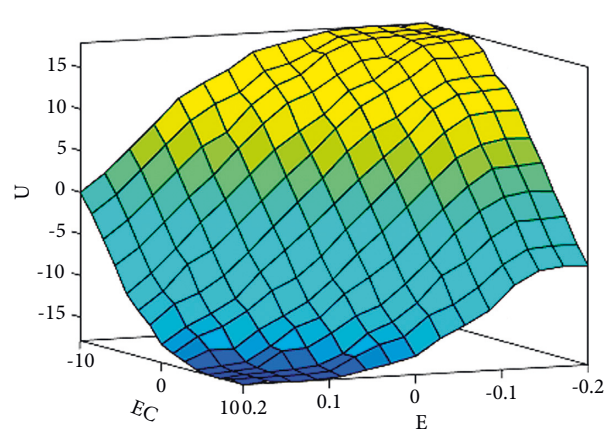

Figure 9: Fuzzy control diagram.

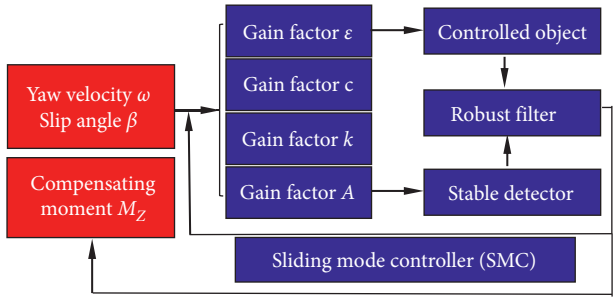

Figure 10: Sliding mode structure controller.

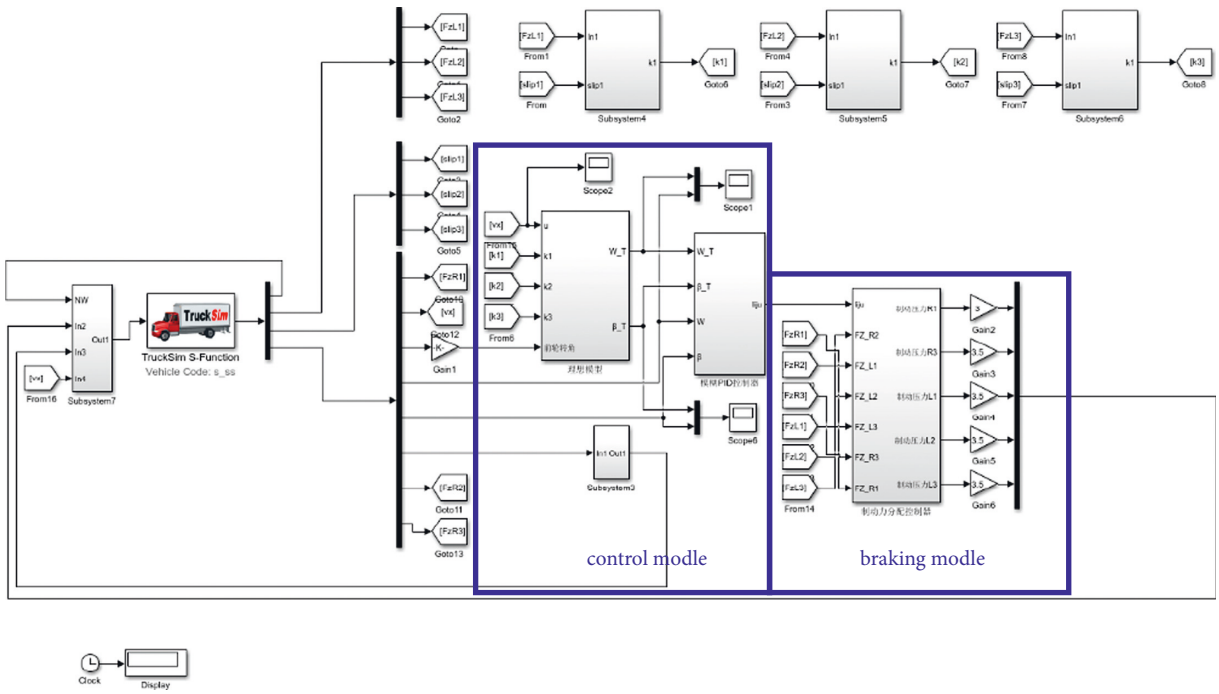

Figure 11: Joint simulation model of vehicle handling stability control.

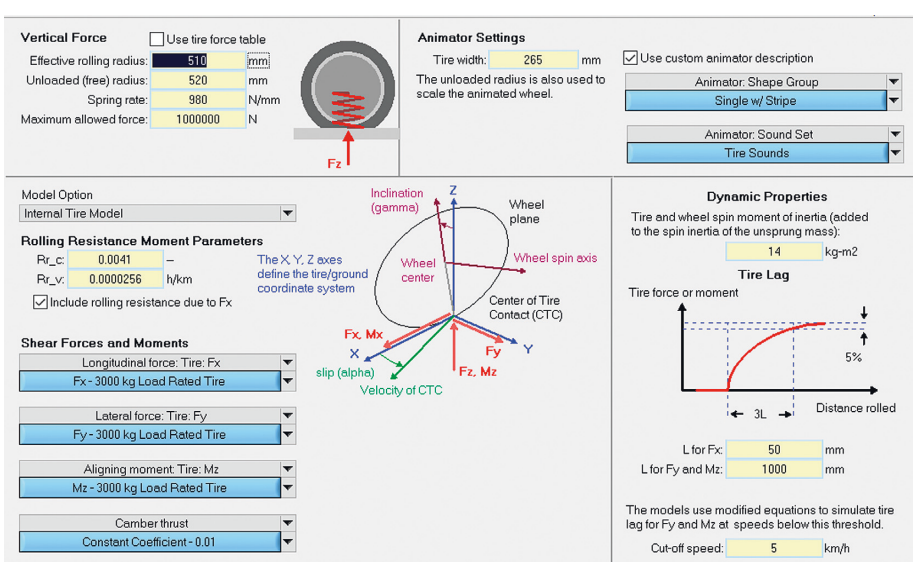

(a)

Figure 12: Continued.

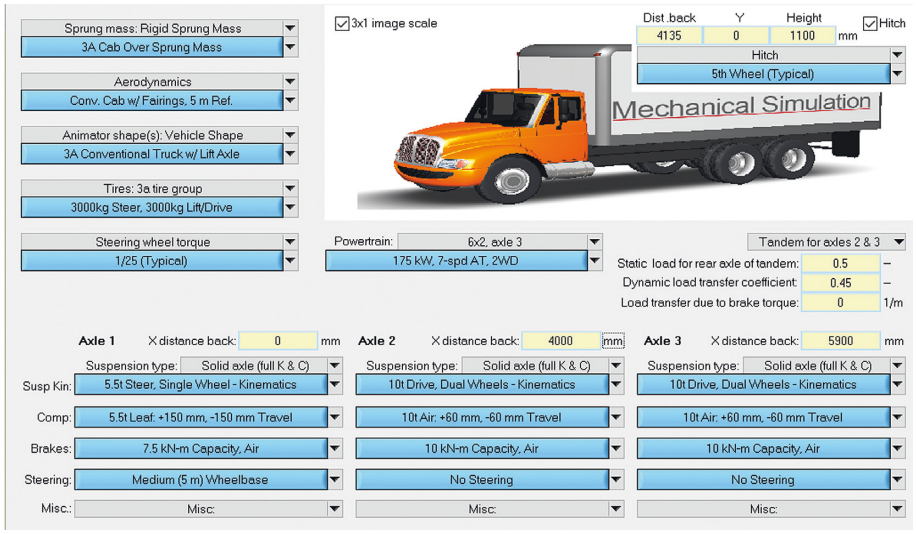

(b)

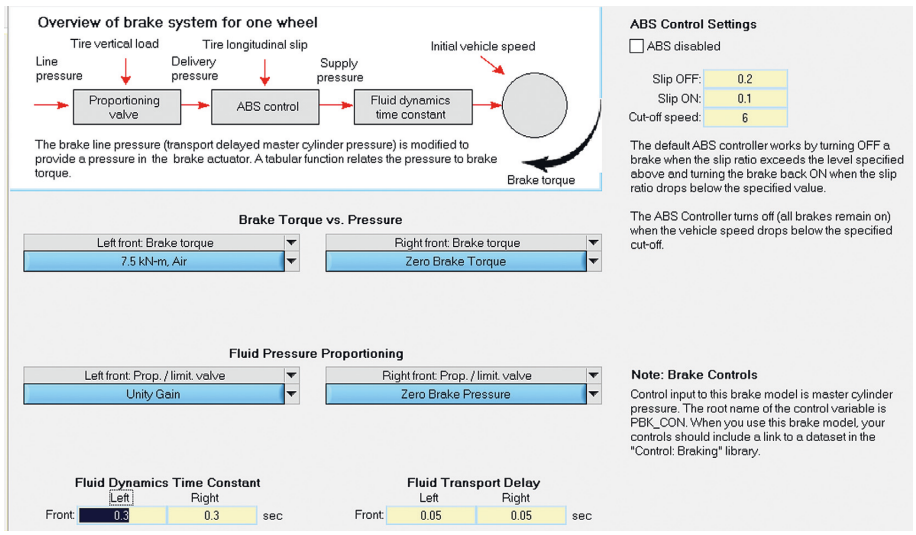

(c)

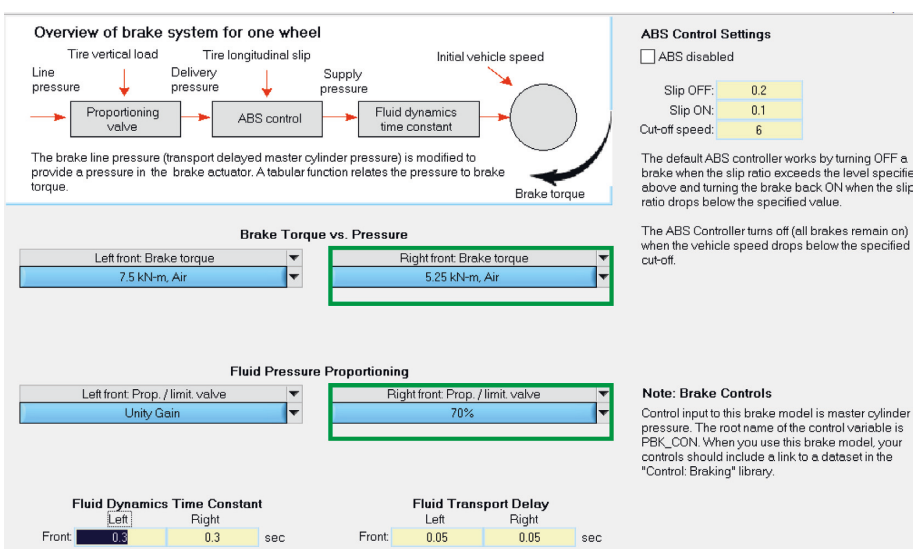

(d)

Figure 12: Multi-body dynamic model diagram. (a) Vehicle tire parameters. (b) Vehicle physical model parameters. (c) Right front wheel complete brake failure model. (d) Incomplete braking failure model of right front wheel.

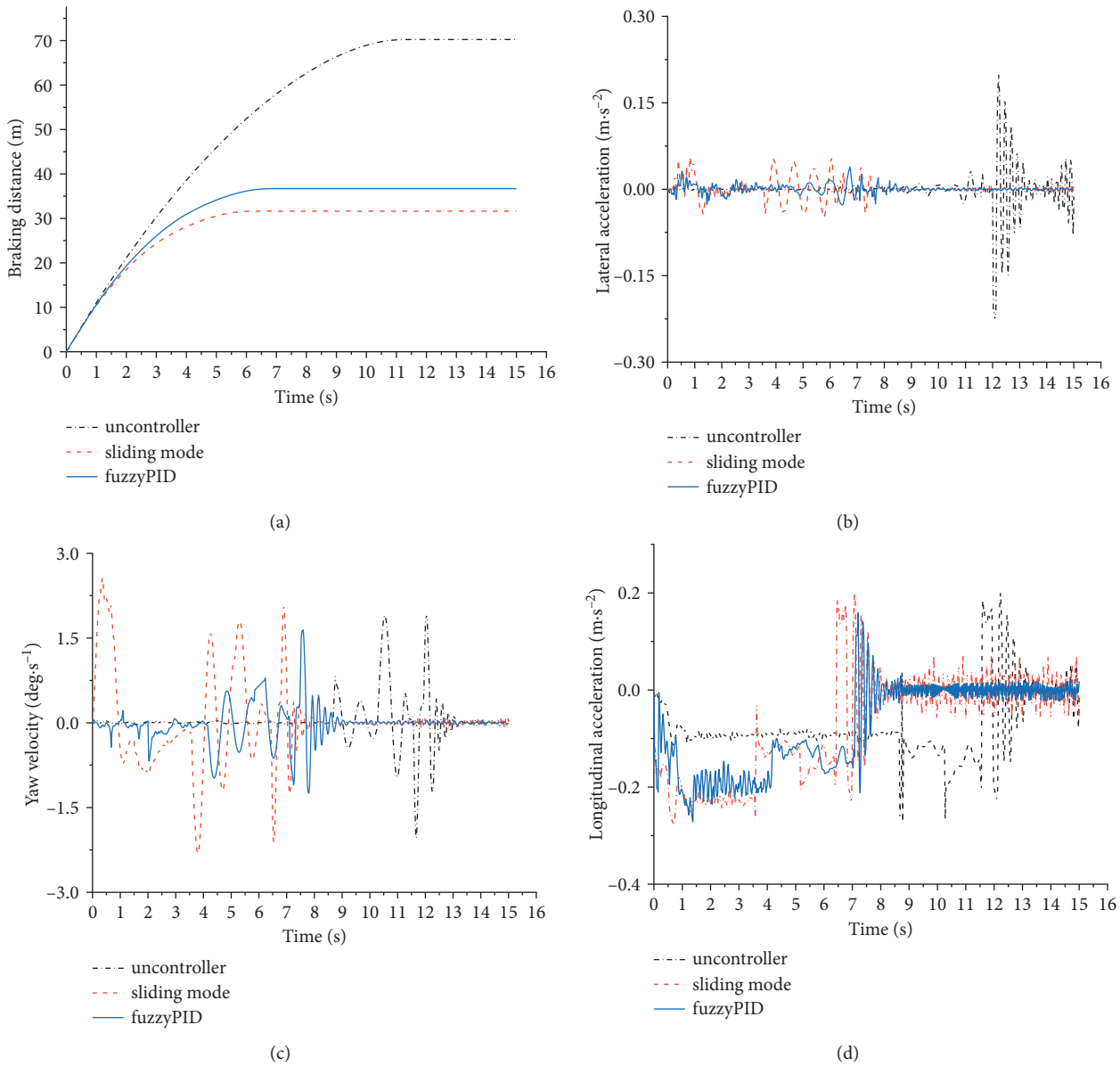

Figure 13: Simulation comparison diagram of different controls in long downhill with $u = 0.5$. (a) Braking distance. (b) Lateral acceleration. (c) Yaw velocity. (d) Longitudinal acceleration.

Because in TruckSim simulation data parameters, braking effectiveness of 50% and 30% in the simulation data parameters are very close, it is difficult to distinguish the change in braking distance and lateral acceleration data, and when the braking efficiency is 30%, the braking degree is close to the complete braking failure. To avoid the accidental repeatability of the data, the braking efficiency 50% is not analyzed.

3. Braking Stability Control Strategy of Heavy Vehicle

3.1. Vehicle Braking Force Distribution Control Strategy. In this section, the braking force distribution of the whole vehicle and the braking force distribution in the case of uncertain failure or failure of the right front wheel are formulated, respectively.

The total braking force is shown as follows:

$$G_x = \frac{\left(F_f + F_m + F_r\right) \cdot g}{W_{01} + W_{02} + W_{03} + W_{04} + W_{05} + W_{06}}, \tag{23}$$

where W_{0i} is the static load of the wheel; F_f, F_m and F_r are the braking forces of the front, middle, and rear axles of the wheel. G is the vehicle gravity.

The braking force of the front, middle, and rear shafts is defined using the function of brake pedal angle, as shown as follows:

$$\begin{cases} F_f = 2K_f \cdot f_v(\theta_b), \\ F_m = 2K_m \cdot f_v(\theta_b), \\ F_r = 2K_r \cdot f_v(\theta_b), \end{cases} \tag{24}$$

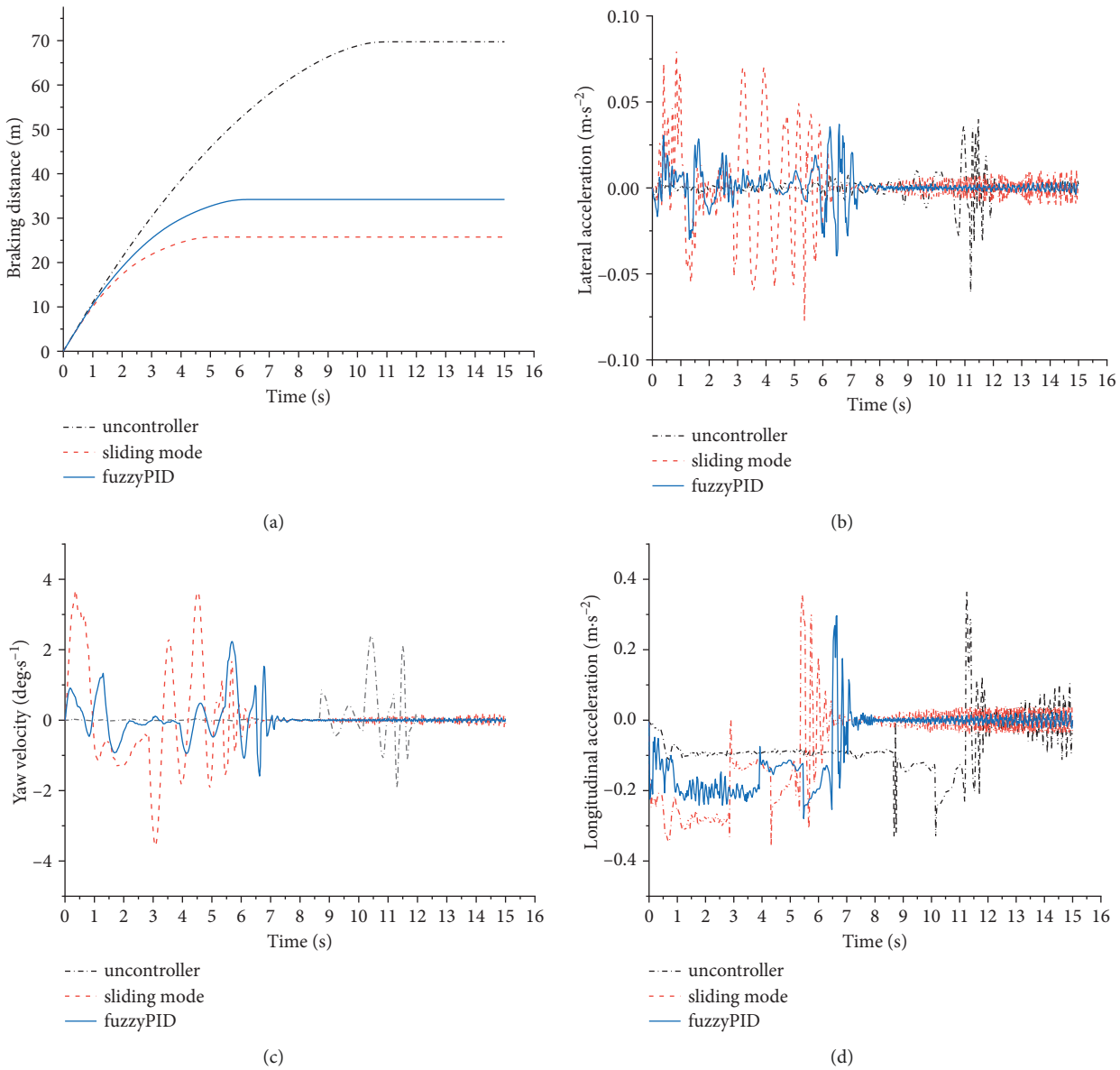

Figure 14: Simulation comparison diagram of different controls in long downhill with $u = 0.7$. (a) Braking distance. (b) Lateral acceleration. (c) Yaw velocity. (d) Longitudinal acceleration.

where f_v is a function of hydraulic nonlinear brake pedal angle in the braking system. K_f, K_m, and K_r are, respectively, the braking characteristic coefficients of the brake, assuming that the relationship between braking force and hydraulic pressure in the braking device is determined in the case of no linear approximation when the wheel is locked.

When the deceleration is set, the target deceleration can be obtained, which can be translated into equation n following equation by substituting

$$G_x = \frac{2\left(K_f + K_m + K_r\right) \cdot g \cdot f_v\left(\theta_b\right)}{W_{01} + W_{02} + W_{03} + W_{04} + W_{05} + W_{06}}. \tag{25}$$

According to the control law 1, the appropriate f_v value is extracted from the experimental results in advance or from the control charts in other literature and experience so that the load conditions $(W_{01} + W_{02} + W_{03} + W_{04} + W_{05} + W_{06})$ do not affect the target deceleration.

Control law 2 determines the braking force assigned to each wheel to prevent uneven wheel locking. This determination factor is based on the dynamic load W_i on each wheel and is calculated by considering the load transfer caused by roll motion and pitch motion. Under the influence of pitching motion, the load on each wheel is described as follows:

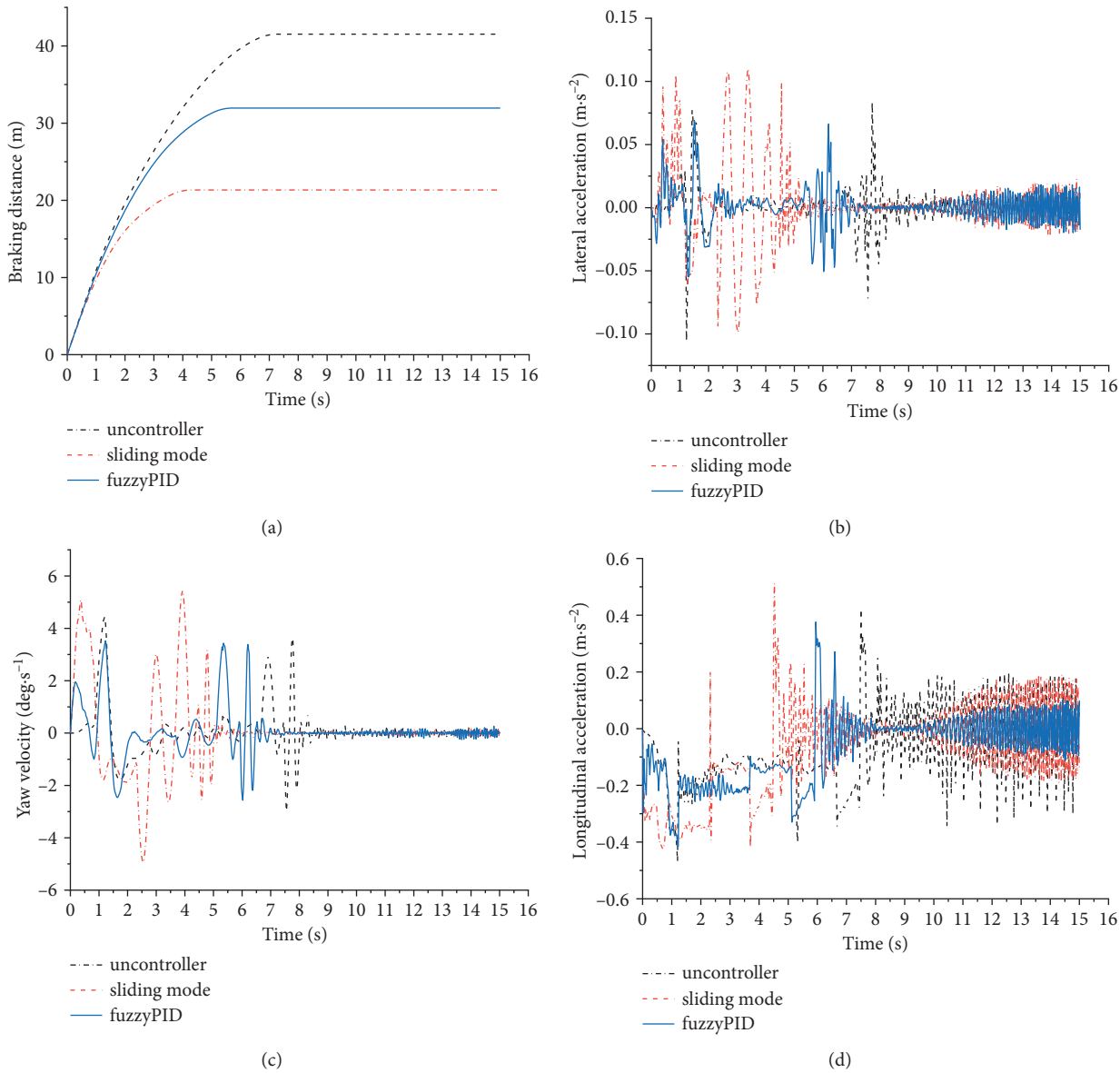

Figure 15: Simulation comparison diagram of different controls in long downhill with $u = 0.9$. (a) Braking distance. (b) Lateral acceleration. (c) Yaw velocity. (d) Longitudinal acceleration.

$$\begin{cases} F_{p1} = F_p + W_{01}, \\ F_{p2} = F_p + W_{02}, \\ F_{p3} = F_p + W_{03}, \\ F_{p4} = F_p + W_{04}, \\ F_{p5} = F_p + W_{05}, \\ F_{p6} = F_p + W_{06}, \end{cases} \tag{26}$$

where F_p is the pitching motion load component, and when the vehicle suddenly brakes or accelerates, the vehicle nose is lifted or tilted down.

The load transfer component caused by pitching motion is shown as follows:

$$\begin{cases} F_p = \dfrac{M_s \cdot G + H_g}{2L}, \\ M_s = \dfrac{W_{01} + W_{02} + W_{03} + W_{04} + W_{05} + W_{06}}{G} - M_{us}, \end{cases} \tag{27}$$

where M_s is the mass of the vehicle spring; M_{us} refers to the unsprung mass of the vehicle, the mass not supported by the elastic components in the suspension system, generally including wheels, springs, and shock absorbers. In practical calculation, 1/2 of the mass of these components is generally taken as the lower spring mass. H_g is the height of the center of gravity. G is the vehicle gravity.

The load transfer components of the front, middle, and rear axles caused by yaw motion are shown as follows:

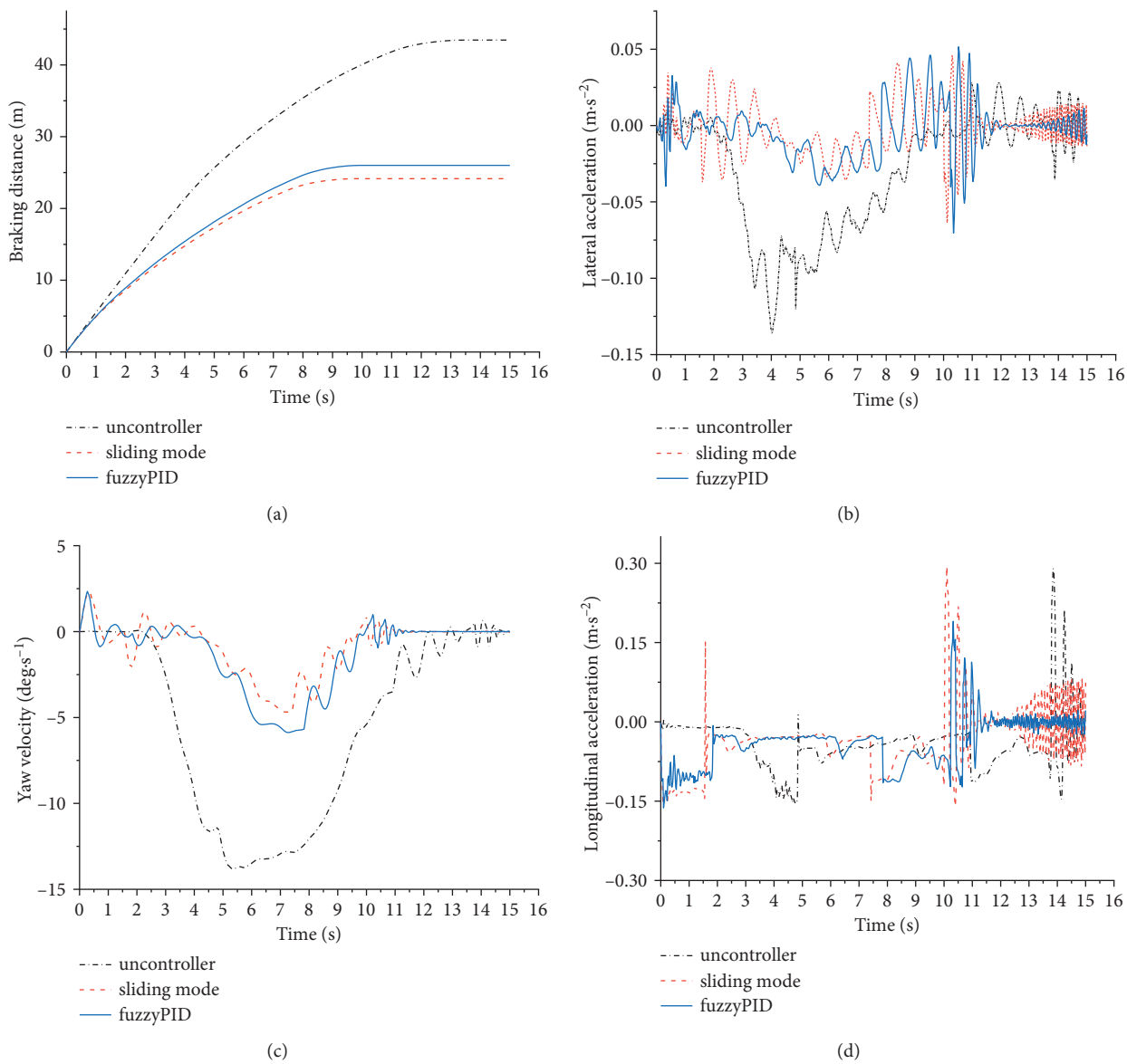

Figure 16: Simulation comparison diagram of different controls in curve driving with $u = 0.5$. (a) Braking distance. (b) Lateral acceleration. (c) Yaw velocity. (d) Longitudinal acceleration.

$$\begin{cases} F_{rf} = \dfrac{(F_{p1} + F_{p2}) \cdot H_G \cdot G_{yf}}{G \cdot T_{sf}}, \\ F_{rm} = \dfrac{(F_{p3} + F_{p4}) \cdot H_G \cdot G_{ym}}{G \cdot T_{sm}}, \\ F_{rr} = \dfrac{(F_{p5} + F_{p6}) \cdot H_G \cdot G_{yr}}{G \cdot T_{sr}}. \end{cases} \tag{28}$$

G_{yf}, G_{ym}, and G_{yr} are the lateral accelerations of the front, middle, and rear axles, respectively. T_{sf}, T_{sm}, and T_{sr} are wheel tread of front axle, middle axle, and rear axle, respectively, that is, the contact part between wheel and ground.

The dynamic load on each wheel during braking is shown as follows:

$$\begin{cases} W_1 = F_{p1} + F_{rf}, \\ W_2 = F_{p2} - F_{rf}, \\ W_3 = F_{p3} + F_{rm}, \\ W_4 = F_{p4} - F_{rm}, \\ W_5 = F_{p5} + F_{rr}, \\ W_6 = F_{p6} - F_{rr}. \end{cases} \tag{29}$$

In this study, the right turn is set, and the lateral acceleration is defined as the positive acceleration on the right side. To balance the centrifugal force, the positive

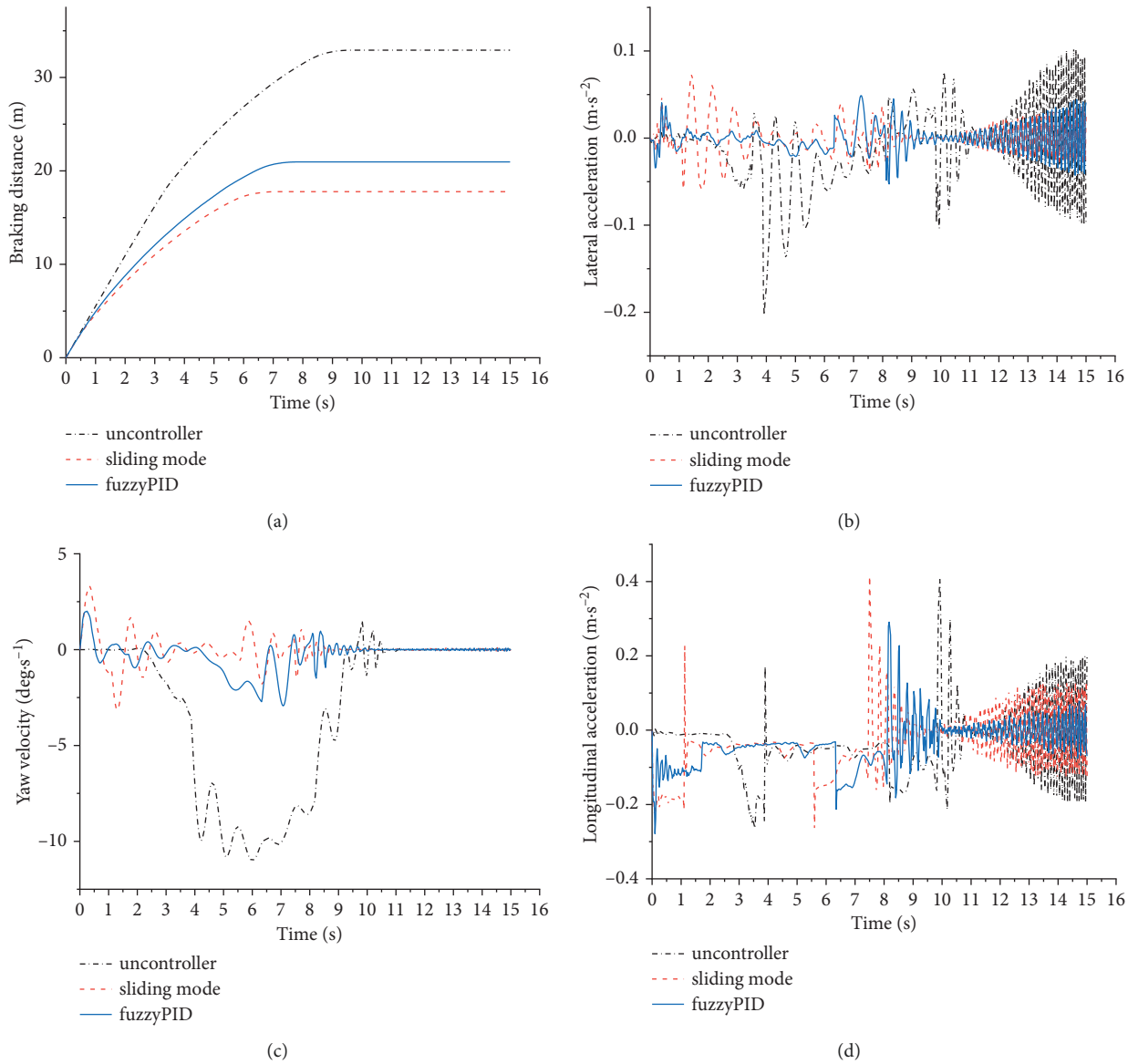

Figure 17: Simulation comparison diagram of different controls in curve driving with $u = 0.7$. (a) Braking distance. (b) Lateral acceleration. (c) Yaw velocity. (d) Longitudinal acceleration.

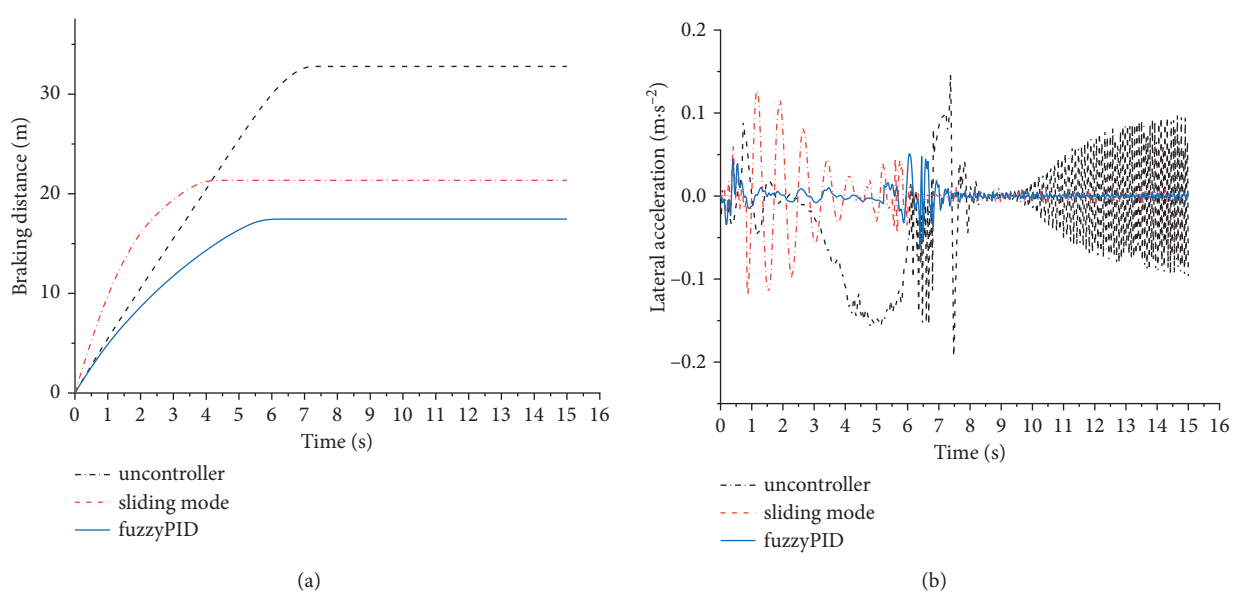

Figure 18: Continued.

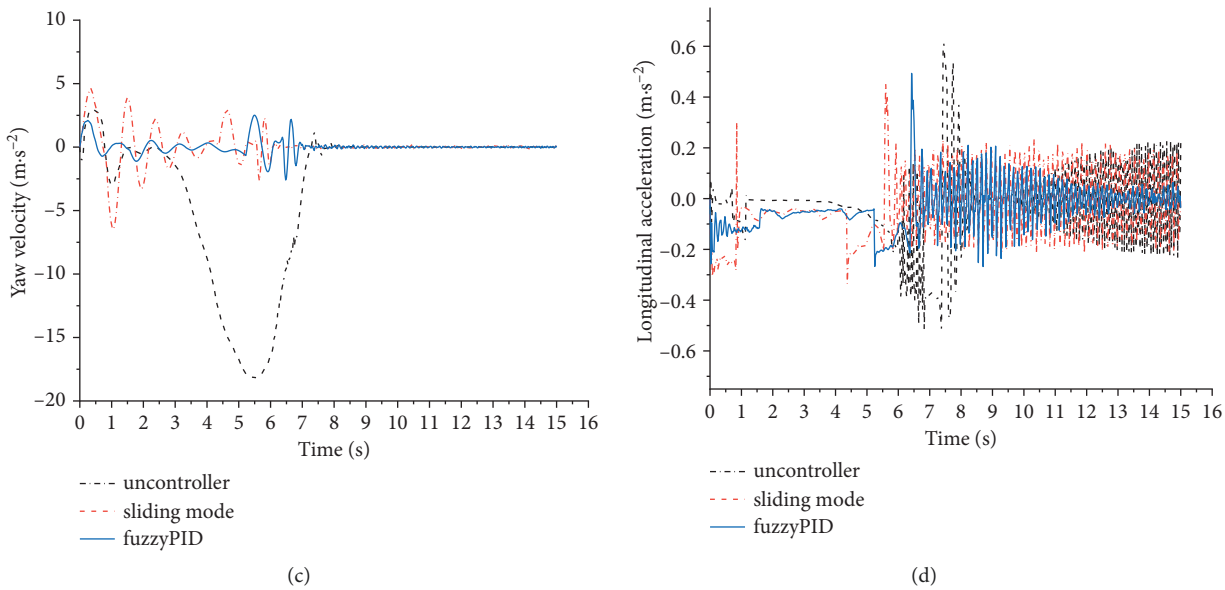

Figure 18: Simulation comparison diagram of different controls in curve driving with $u = 0.9$. (a) Braking distance. (b) Lateral acceleration. (c) Yaw velocity. (d) Longitudinal acceleration.

increased load component is given when the left brakes, while the centrifugal force of the inner wheel is relatively small. To maintain force balance, the load component is reduced.

The target braking force of each wheel is calculated according to control law 2, as shown as follows:

$$\begin{cases} F_{b1} = \dfrac{W_1}{W_1 + W_2} F_f, \\ F_{b2} = \dfrac{W_2}{W_1 + W_2} F_f, \\ F_{b3} = \dfrac{W_3}{W_3 + W_4} F_m, \\ F_{b4} = \dfrac{W_4}{W_3 + W_4} F_m, \\ F_{b5} = \dfrac{W_5}{W_5 + W_6} F_r, \\ F_{b6} = \dfrac{W_6}{W_5 + W_6} F_r, \end{cases} \tag{30}$$

where F_f, F_m, and F_r are braking forces of the front bridge, middle bridge, and rear bridge, respectively.

The target pressure of each actuator is shown as follows:

$$\begin{cases} P_{a1} = f_a\left(\dfrac{F_{b1}}{K_f}\right), \\ P_{a2} = f_a\left(\dfrac{F_{b2}}{K_f}\right), \\ P_{a3} = f_a\left(\dfrac{F_{b3}}{K_f}\right), \\ P_{a4} = f_a\left(\dfrac{F_{b4}}{K_f}\right), \\ P_{a5} = f_a\left(\dfrac{F_{b5}}{K_r}\right), \\ P_{a6} = f_a\left(\dfrac{F_{b6}}{K_f}\right), \end{cases} \tag{31}$$

where f_a is the characteristic function of the brake actuator.

The braking force distribution diagram based on the right front wheel of the vehicle is shown in Figure 4, which is mainly reflected in the auxiliary effect on the vehicle braking force distribution.

F_k is the force transferred from the pressure of the pneumatic brake chamber to the brake shoe; F_s is the force transferred from the braking force of the brake shoe to the brake drum; F_{BR} is the force transferred from the brake drum to the wheel; and F_{BT} is the friction braking force generated by contact.

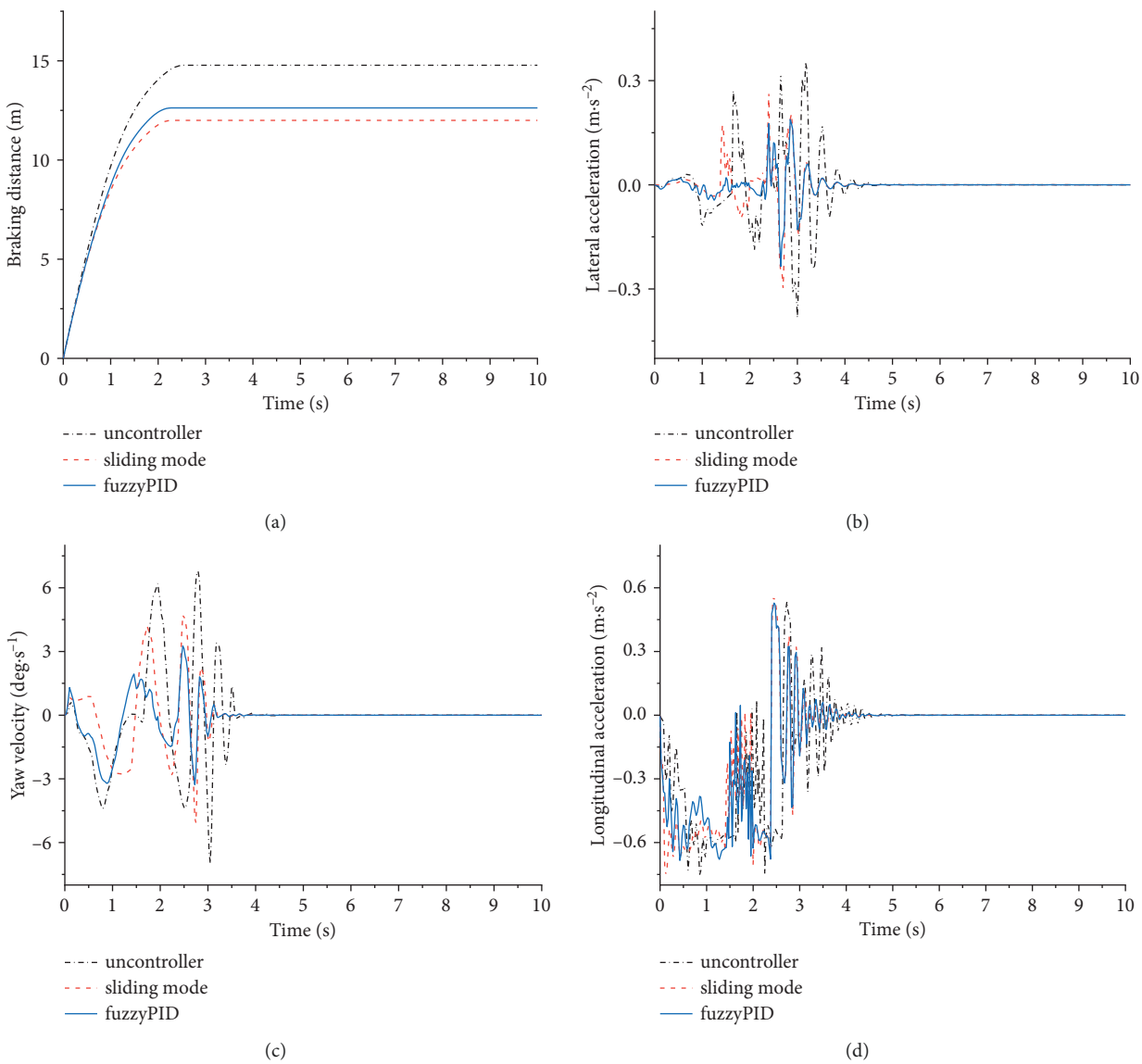

Figure 19: Simulation diagram of curve driving with long downhill braking efficiency of 100% at $u = 0.75$. (a) Braking distance. (b) Lateral acceleration. (c) Yaw velocity. (d) Longitudinal acceleration.

The equation for the ideal braking force of front, middle, and rear wheels can be applied as follows:

$$\begin{cases} F_B = \mu mg, \\ \Delta F = \dfrac{mah}{[L_1 + L_2 + (L_3/2)]}, \\ F_B = F'_{Bf} + F'_{Br1} + F'_{Br2}, \\ F'_{Bf} = (\Delta F + F_f)\mu, \\ F'_{Br1} = (F_{r1} - 0.5\Delta F)\mu, \\ F'_{Br2} = (F_{r2} - 0.5\Delta F)\mu. \end{cases} \tag{32}$$

Among them, $L_1 = 4657$ mm, $L_2 = 2274$ mm, and $L_3 = 1387$ mm; center of gravity height $H = 3484$ mm; reaction force of the front axle, middle axle, and rear axle of vehicle $F_f = 43949$N, $F_{r1} = 79853$ N, and $F_{r2} = 42968$ N; $G = 9.8$ m/s^2; road adhesion coefficient μ depends on the actual situation; and vehicle mass $m = 15000$ kg.

3.2. Control Strategy for Heavy Vehicle

3.2.1. Fuzzy PID Control Strategy. Fuzzy PID control is a widely used control strategy in literature research. Fuzzy control is relatively free and does not require accurate modelling. It can also compensate the zero and blind points generated by PID control. Therefore, this study combines PID controller with fuzzy controller, both simulation analysis and hardware-in-the-loop verification have

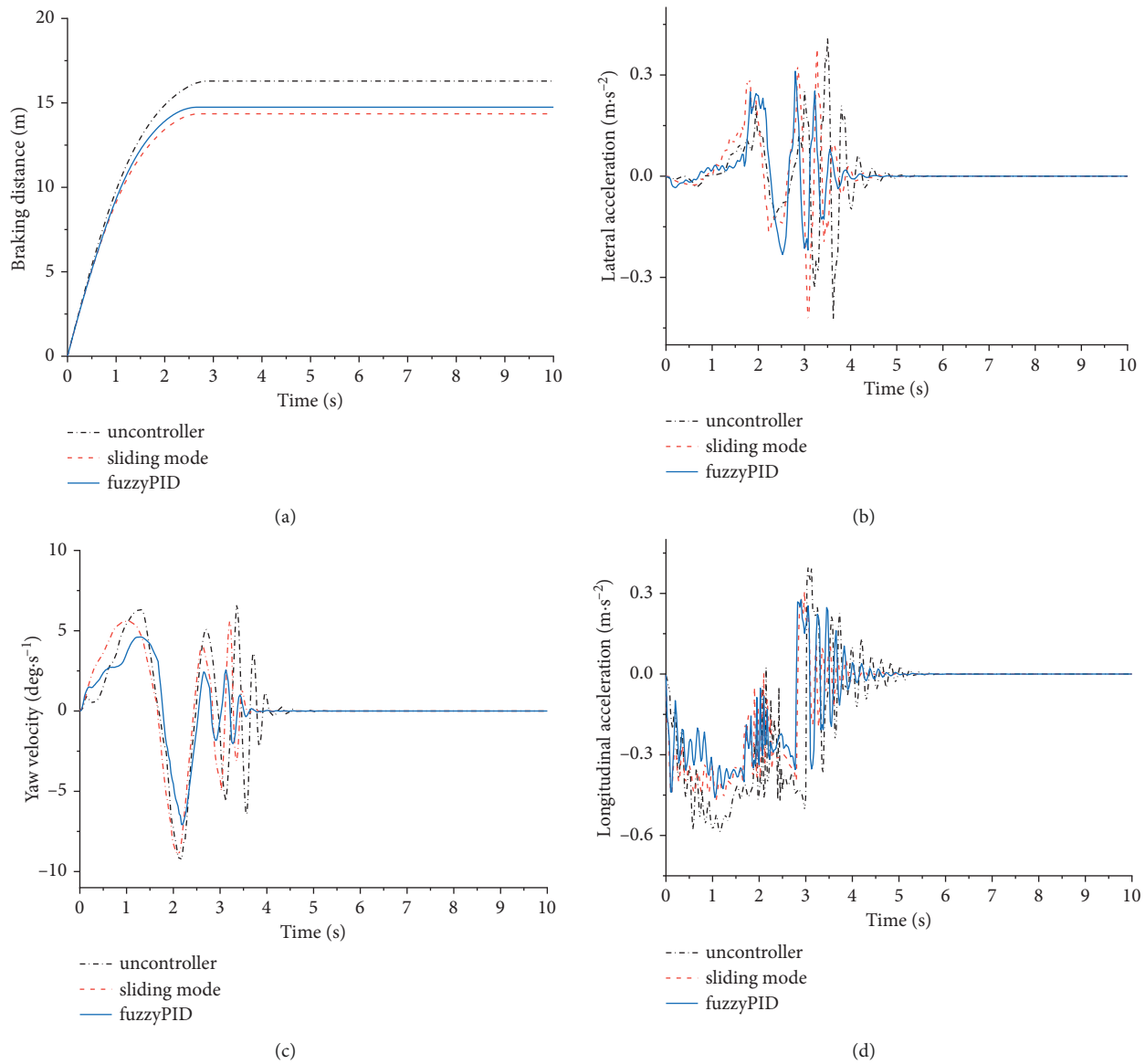

Figure 20: Simulation diagram of curve driving with long downhill braking efficiency of 70% at $u = 0.75$. (a) Braking distance. (b) Lateral acceleration. (c) Yaw velocity. (d) Longitudinal acceleration.

achieved good control results, and the diagram of fuzzy PID controller is shown in Figure 5.

According to the design of fuzzy controller, the fuzzy sets of input variable deviation E, deviation change rate EC, and output variable U are as follows: {NB, NM, NS, ZO, PS, PM, PB}, respectively, represent negative large (NB), negative medium (NM), negative small (NS), zero (ZO), positive small (PS), median (PM), and cp (PB). The choice of the numerical range of the field is based on simulation results and is determined according to various literature experiences. The domain of E is [−6, 6], the domain of EC is [−10, 10], and the domain of U is [−1, 1]. The fuzzy rules are shown in Table 2.

In this study, the yaw velocity error of input variables, sideslip error of centroid, and yaw compensation moment of output variables are all adopted Gaussian membership function, and the membership function of input variables and output variables is shown in Figures 6–9.

3.2.2. Sliding Mode Control Strategy for Heavy Vehicle. An important advantage of sliding mode control is robustness. When the system is in a sliding model, it has excellent insensitivity to the model error of the controlled object, the change in object parameters, and external interference. Compared with PID fuzzy control, sliding mode control has a faster response time and is less sensitive to the disturbance of parameter changes, and does not require online identification of the system. Therefore, adding sliding mode control to the braking system can effectively shorten the braking distance of the vehicle compared with PID fuzzy

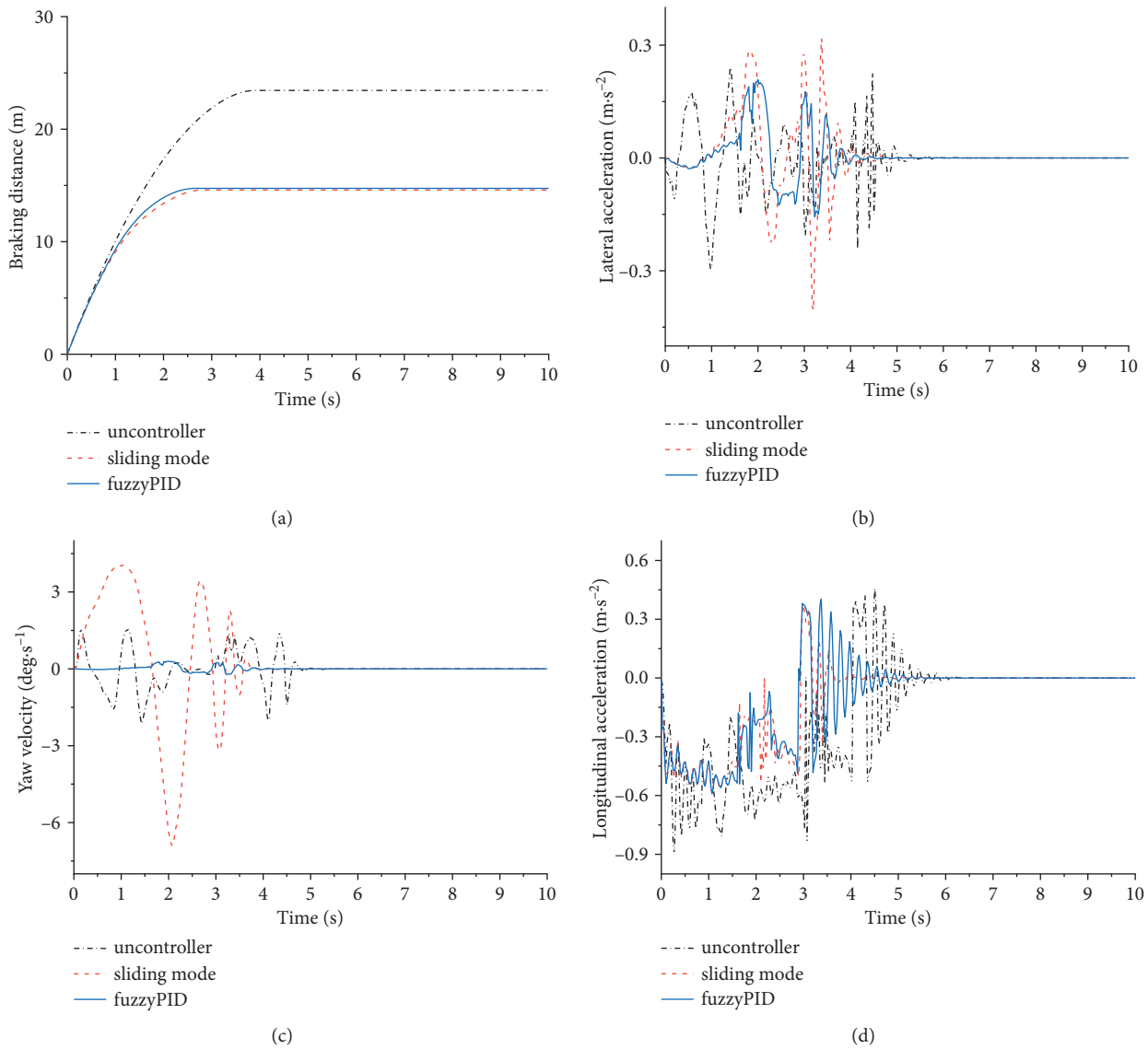

Figure 21: Simulation diagram of curve driving with long downhill braking efficiency of 50% at $u = 0.75$. (a) Braking distance. (b) Lateral acceleration. (c) Yaw velocity. (d) Longitudinal acceleration.

control. However, its lateral control effect is poor, so the suitable sliding film control is more suitable for straight-line braking. Its working principle is shown in Figure 10 and in the following equation.

$$i_q = \frac{1}{A}\int (cx_2 + \varepsilon \cdot \sin s + ks)dt. \tag{33}$$

In the Simulink sliding mode controller, four gain coefficients ε, K, C, and A are set, and the braking control is regulated by adjusting the gain coefficients. Sliding mode control has been widely used mainly because of its good control performance for nonlinear systems, its applicability for multiple-input multiple-output systems, and the establishment of good design standards for discrete time systems.

3.3. Modelling of Control Strategy. According to the fuzzy PID control and sliding mode control models established above, as shown in Figure 11, the Simulink braking torque distribution module and control module of the three-axis heavy vehicle are established based on the vehicle dynamic model of complete braking failure and uncertain braking failure. For the vehicle dynamic model, TruckSim's main input is left and right wheel cylinder pressure of front axle, middle axle, and rear axle, and its output is longitudinal force, longitudinal speed, front wheel angle, yaw angle, and slip rate.

According to the TruckSim vehicle analysis, the parameters of a heavy-duty vehicle of Dongfeng series are brought into TruckSim. Later, braking force parameters, equal length downhill slope of vehicle model, and curve conditions will be set in TruckSim. Multi-body dynamic operation is shown in Figure 12.

Taking the yaw moment coefficient as an example, its parameter principle and aerodynamic effect are expressed as force and moment vectors acting on sprung mass points in

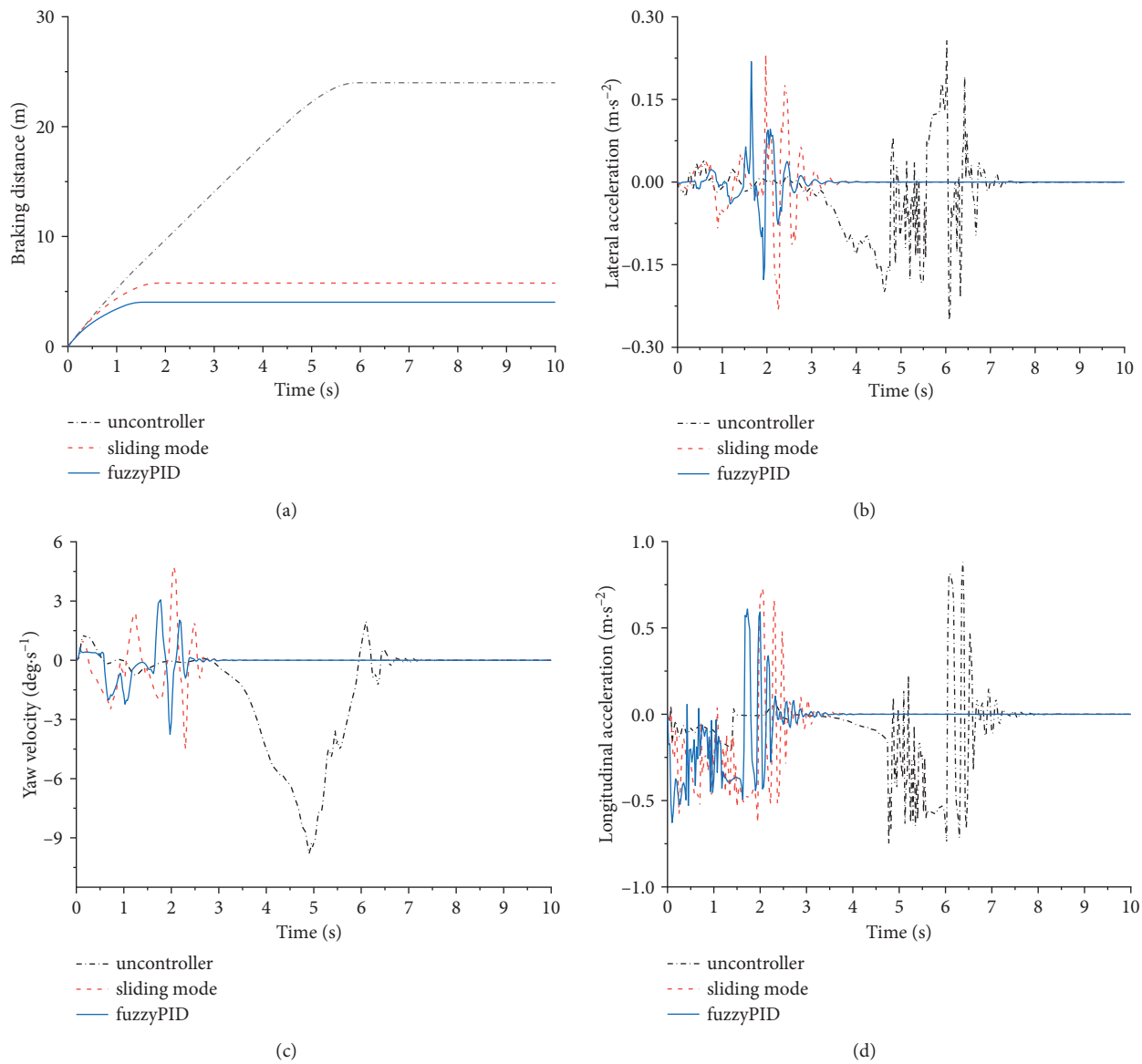

Figure 22: Simulation diagram of curve driving with braking efficiency of 100% at $u = 0.75$. (a) Braking distance. (b) Lateral acceleration. (c) Yaw velocity. (d) Longitudinal acceleration.

vehicle models. Each vector consists of three components (X, Y, and Z) parallel to the axis of the sprung mass coordinate system. The three force components are shown by dimensionless coefficients C_1 and C_2, aerodynamic cross-sectional area A, and dynamic pressure Q, defined in the following equations:

$$F = C_1 \cdot C_2 \cdot Q \cdot A, \tag{34}$$

$$Q = \frac{\rho V^2}{2}, \tag{35}$$

where $\rho = 1.206\,\mathrm{kg/m^3}$ is the air density and V is the speed of the air relative to the vehicle. The coefficients C_1 and C_2 differ in the three force directions. One is a function of aerodynamic slip angle, and the other is a function of vehicle chassis height. The three moments of vehicle centroid due to force depend on the position of aerodynamic reference points.

Therefore, the general form of the torque equation is similar to

$$M = C_1 \cdot C_2 \cdot Q \cdot L \cdot A, \tag{36}$$

where L is the vehicle body length.

3.4. Control Analysis of Complete Braking Failure. In this section, the braking stability of heavy vehicles under downhill and curve driving conditions is analyzed, and the non-sliding mode or fuzzy PID control and sliding mode control are compared under different road adhesion coefficients, and the simulation is shown in Figures 13–18.

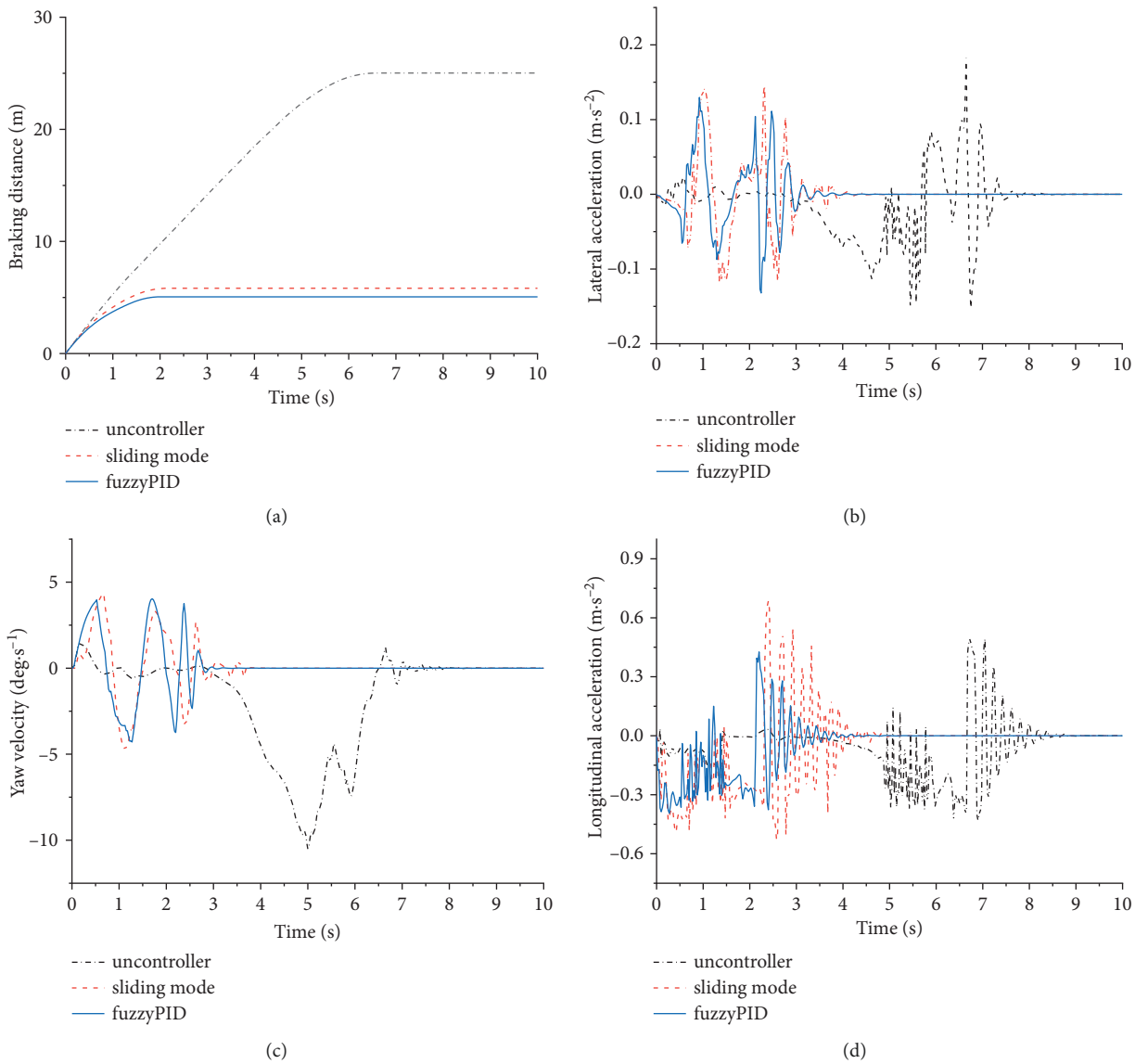

Figure 23: Simulation diagram of curve driving with braking efficiency of 70% at $u = 0.75$. (a) Braking distance. (b) Lateral acceleration. (c) Yaw velocity. (d) Longitudinal acceleration.

The simulation of vehicle right front wheel braking failure under different road adhesion coefficients shows that the fuzzy PID control has a longer braking distance than the sliding mode control, but it performs better in operation stability. It is better to choose vehicle braking control as fuzzy PID control strategy in long downhill road conditions.

From the simulation of the complete braking failure of the right front wheel of the vehicle under different road adhesion coefficients, it can be seen that under the curve driving condition, the fuzzy PID control still performs better than the sliding mode control in the operation stability.

Taking longitudinal acceleration as an example, the multi-body dynamic simulation is set to start braking from 0 s. When the initial value is 0 s, there is an initial vehicle downhill speed of 40 km/h and the curve driving speed of 20 km/h. The vehicle brakes and decelerates from 0 seconds. In the first few seconds, the longitudinal acceleration of the vehicle is greater than that of the vehicle without control. The longitudinal acceleration of the vehicle with control mode improves better with the extension of braking time. The vehicle brakes in time and the longitudinal acceleration decreases.

3.5. Control Analysis of Interval Uncertain Braking Failure. To quantitatively analyze the influence of road adhesion coefficient and uncertain braking torque on vehicle braking stability under special working conditions, the compensation control strategy under uncertain braking failure is designed for single-wheel braking. The co-simulation was carried out by TruckSim-Simulink software, and the simulation analysis was carried out under different braking torque and braking distribution ratios, and the simulation is shown in Figures 19–24.

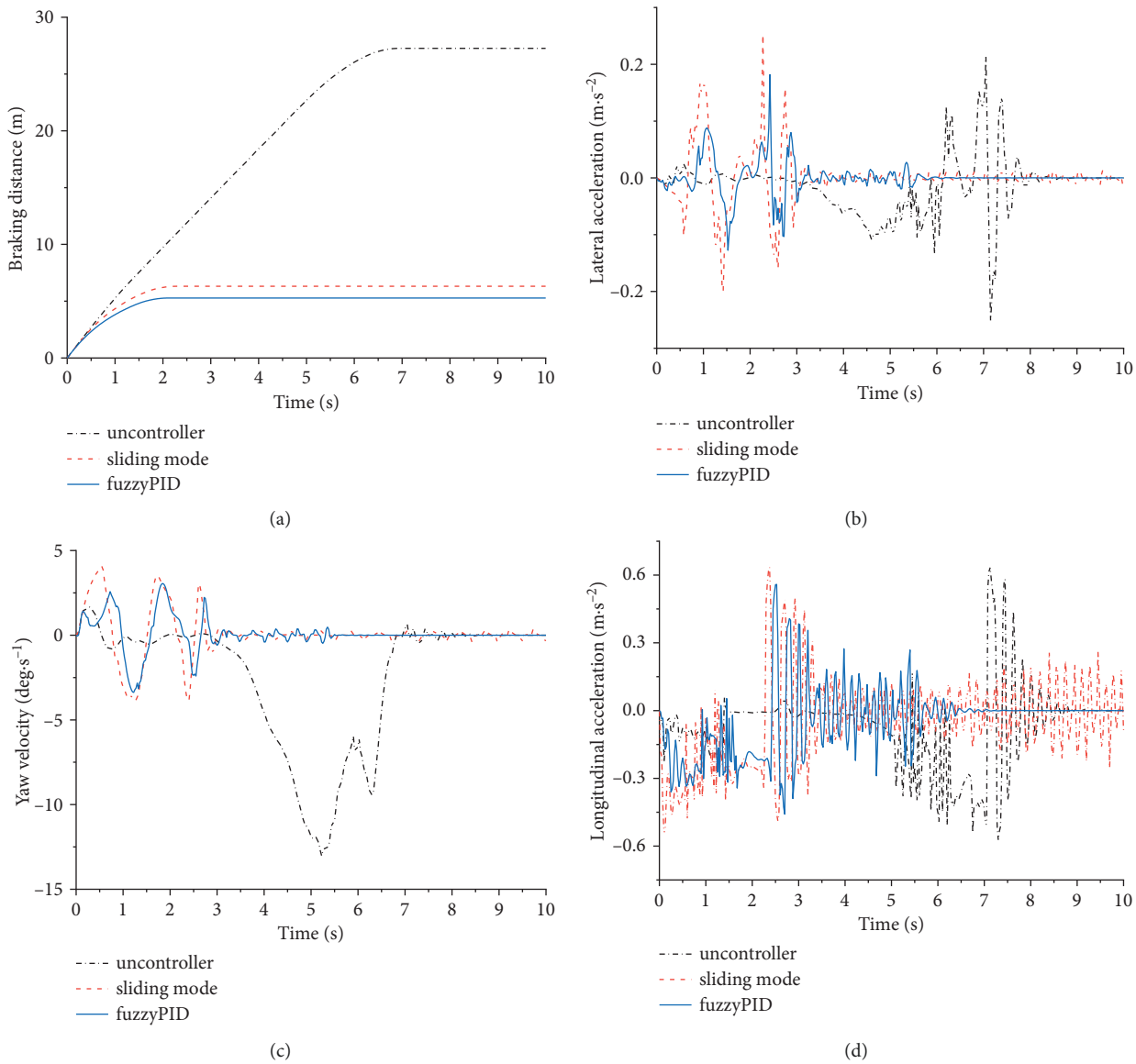

Figure 24: Simulation diagram of curve driving with braking efficiency of 50% at $u = 0.75$. (a) Braking distance. (b) Lateral acceleration. (c) Yaw velocity. (d) Longitudinal acceleration.

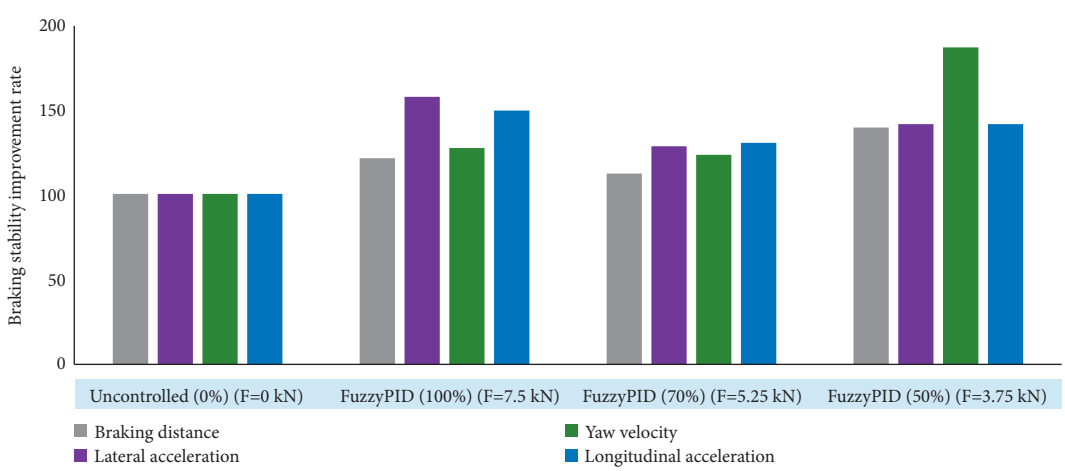

Figure 25: Fuzzy PID control in different braking efficiency improvements.

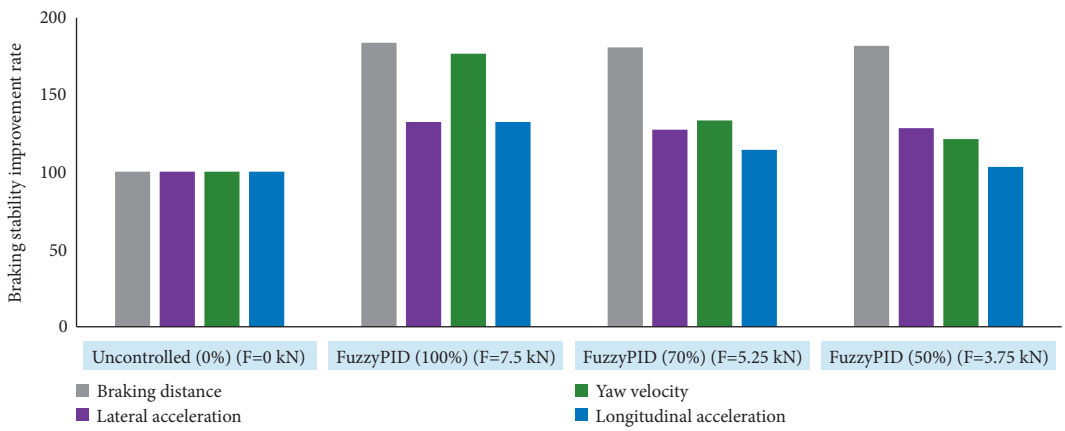

Figure 26: Fuzzy PID control in different braking efficiency improvements.

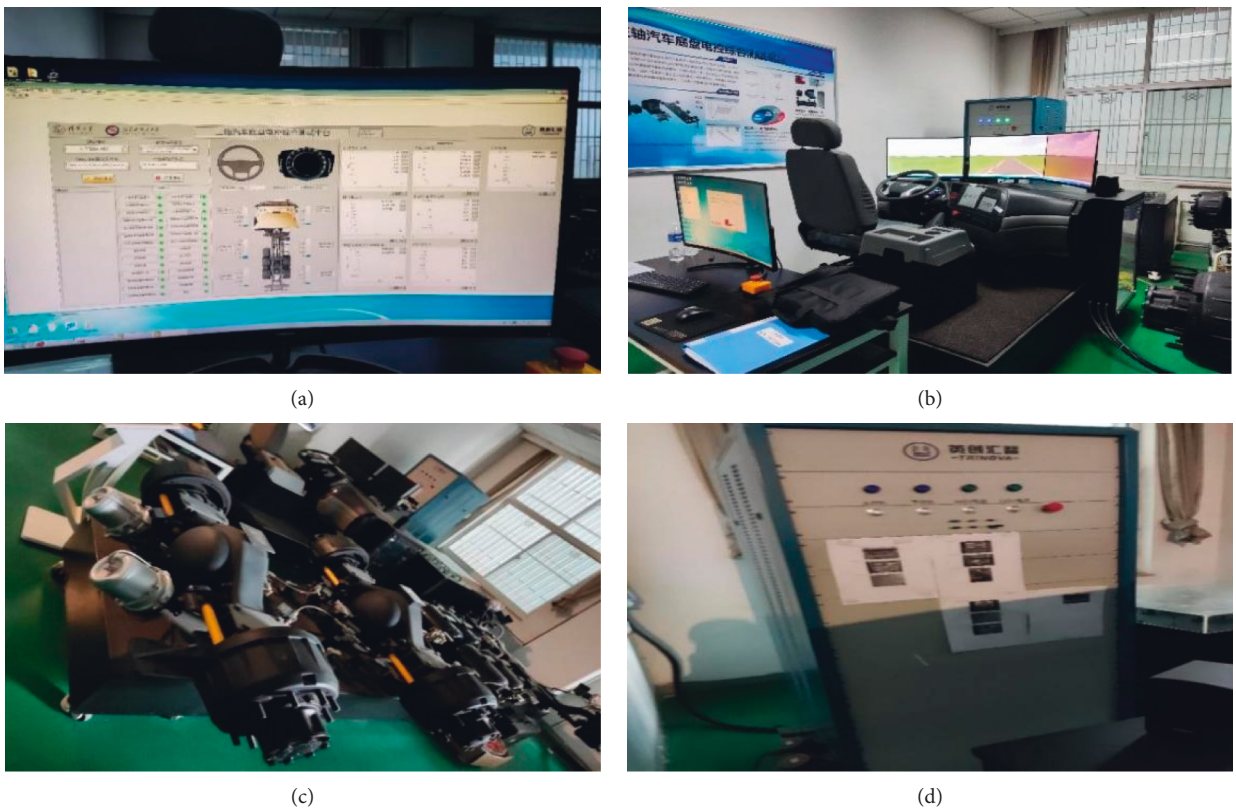

Figure 27: Operational physical map of HIL platform. (a) Hardware test platform. (b) Hardware experimental driving simulator. (c) Dongfeng three-axle chassis. (d) Hardware electrical cabinet.

Based on the fuzzy PID control, the improvement rate is obtained from the comparison between the simulation data and the uncontrolled data as shown in the following figure. To show the histogram clearly, the braking efficiency without control mode is set to 100%, and the improvement rate under fuzzy PID control is regarded as positive improvement relative to that without control if it is higher than 100%. If the improvement rate is less than 100%, it is regarded as a reverse improvement, which has not been improved. The maximum improvement rate is shown in Figure 25.

The vehicle runs on a curved road with a specific road adhesion coefficient of 0.75. It can be seen from the simulation diagram that the fuzzy PID control is still more stable than the sliding mode control on the whole. The maximum improvement rate is shown in Figure 26.

4. HIL Experiment Verification

4.1. HIL Equipment. HIL is hardware in loop test. The hardware-in-the-loop experimental platform is developed jointly with Tsinghua University. The HIL experimental

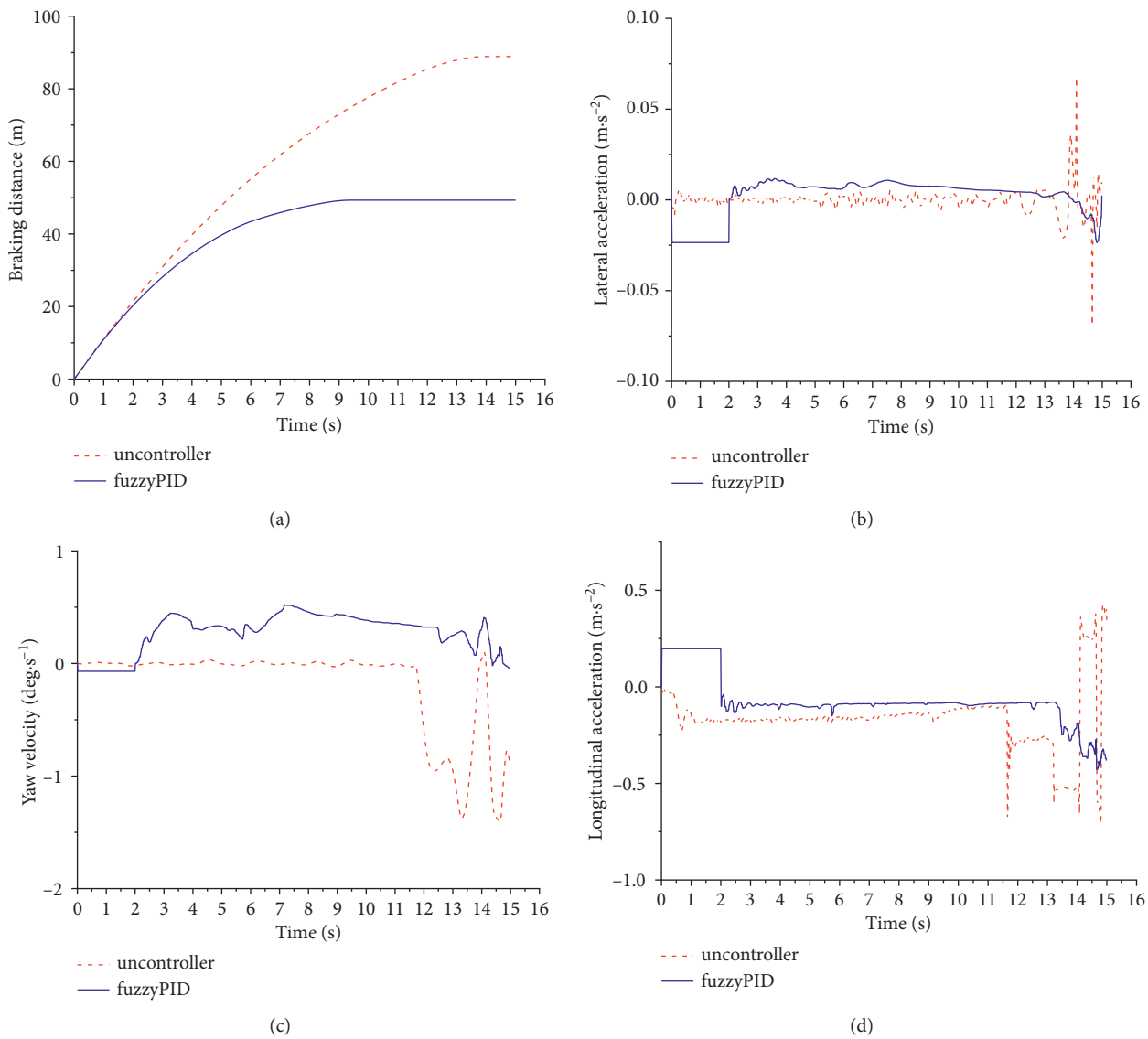

Figure 28: HIL test diagram under long downhill condition when $u = 0.4$. (a) Braking distance. (b) Lateral acceleration. (c) Yaw velocity. (d) Longitudinal acceleration.

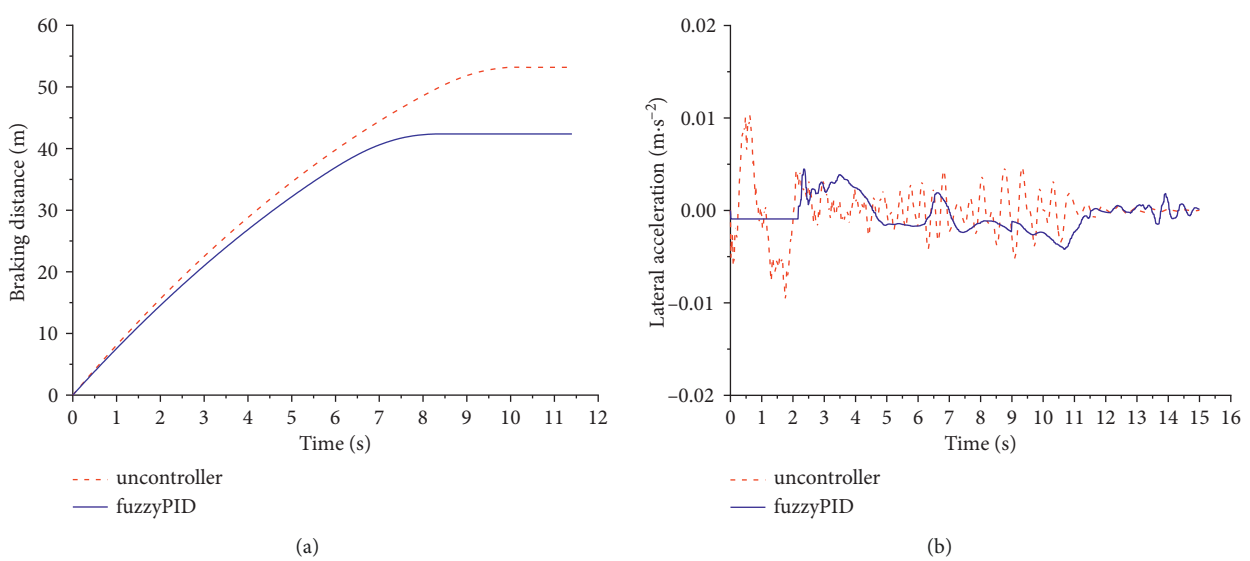

Figure 29: Continued.

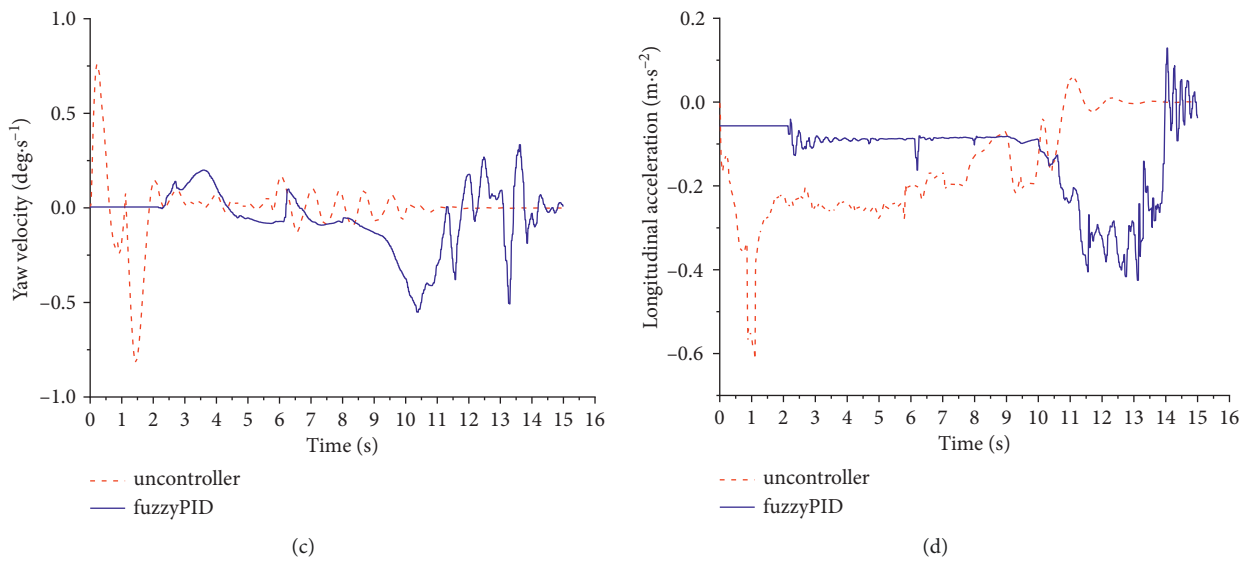

Figure 29: HIL test diagram under long downhill condition when $u = 0.5$. (a) Braking distance. (b) Lateral acceleration. (c) Yaw velocity. (d) Longitudinal acceleration.

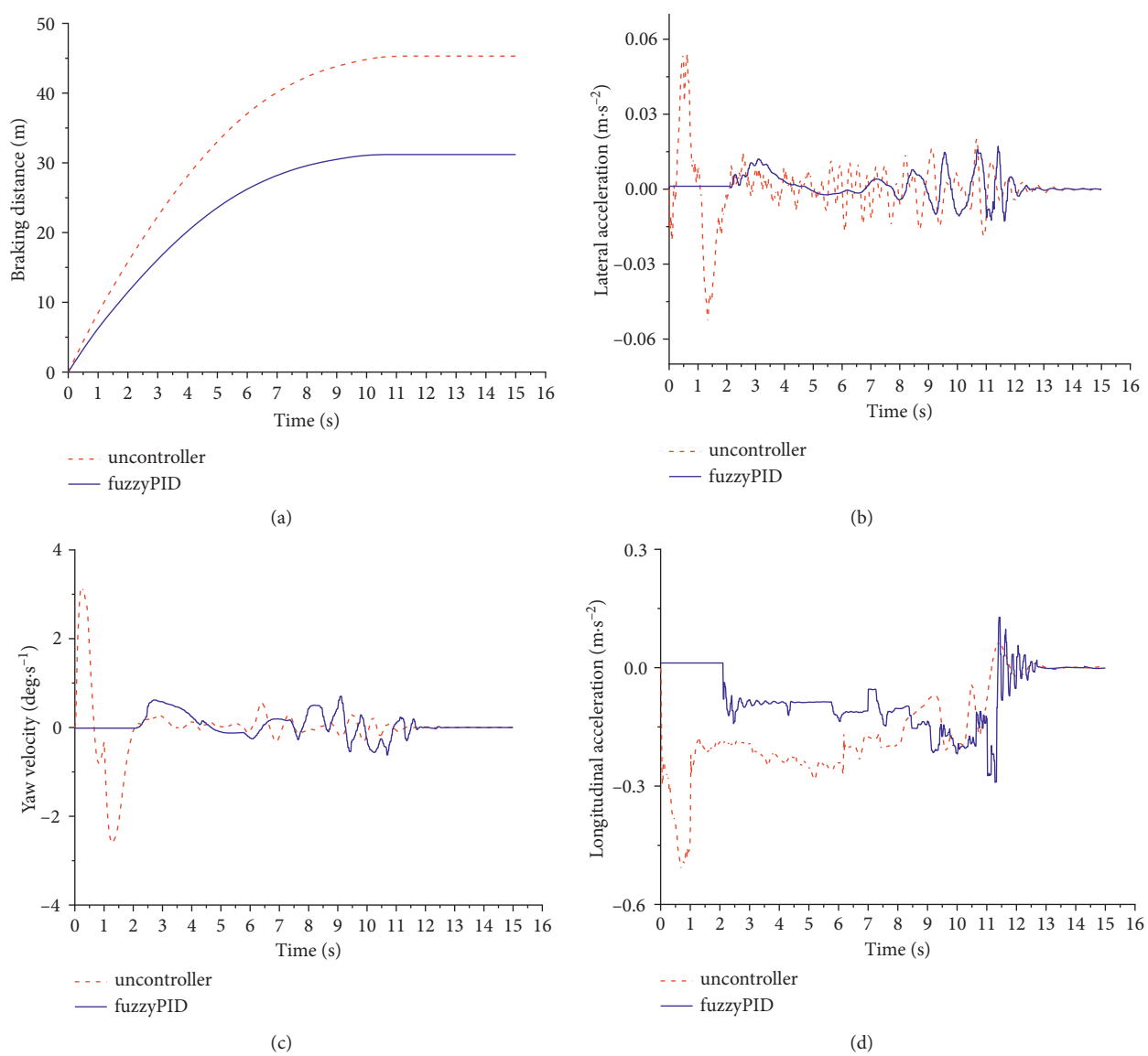

Figure 30: HIL test diagram under long downhill condition when $u = 0.8$. (a) Braking distance. (b) Lateral acceleration. (c) Yaw velocity. (d) Longitudinal acceleration.

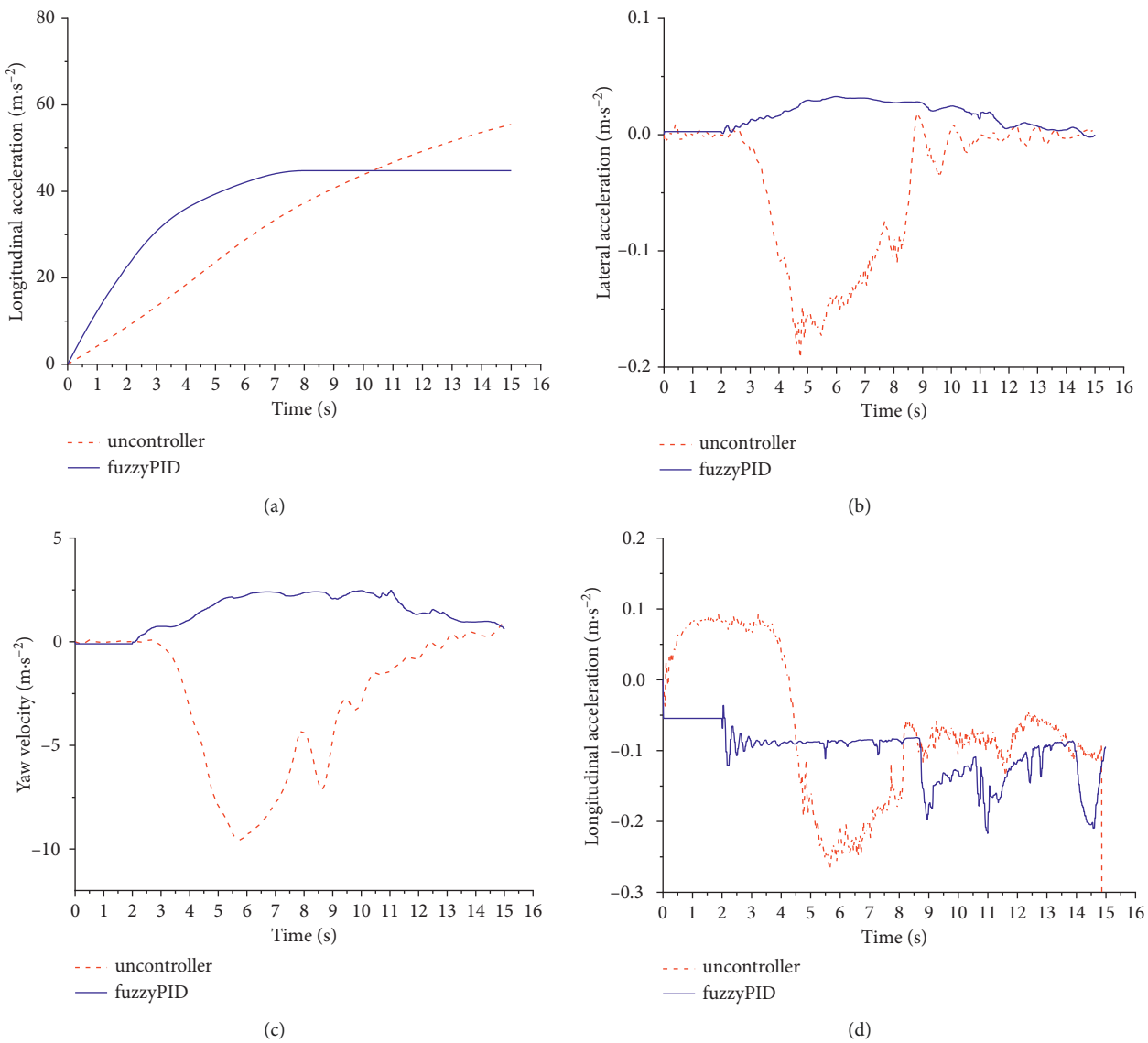

Figure 31: HIL test diagram under curve operating conditions when $u = 0.4$. (a) Braking distance. (b) Lateral acceleration. (c) Yaw velocity. (d) Longitudinal acceleration.

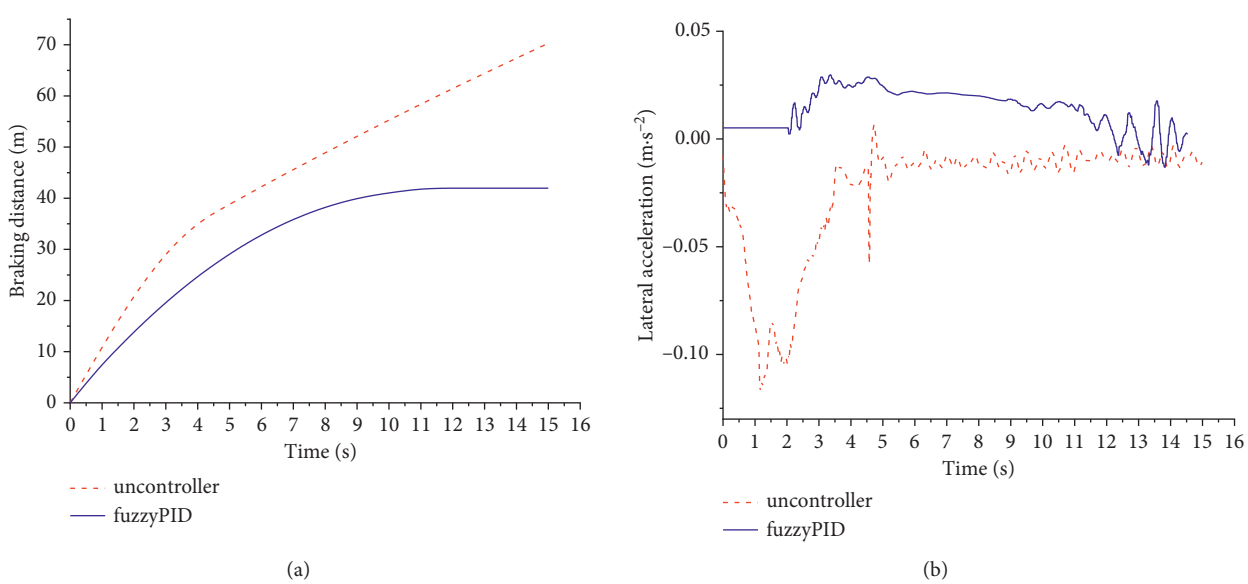

Figure 32: Continued.

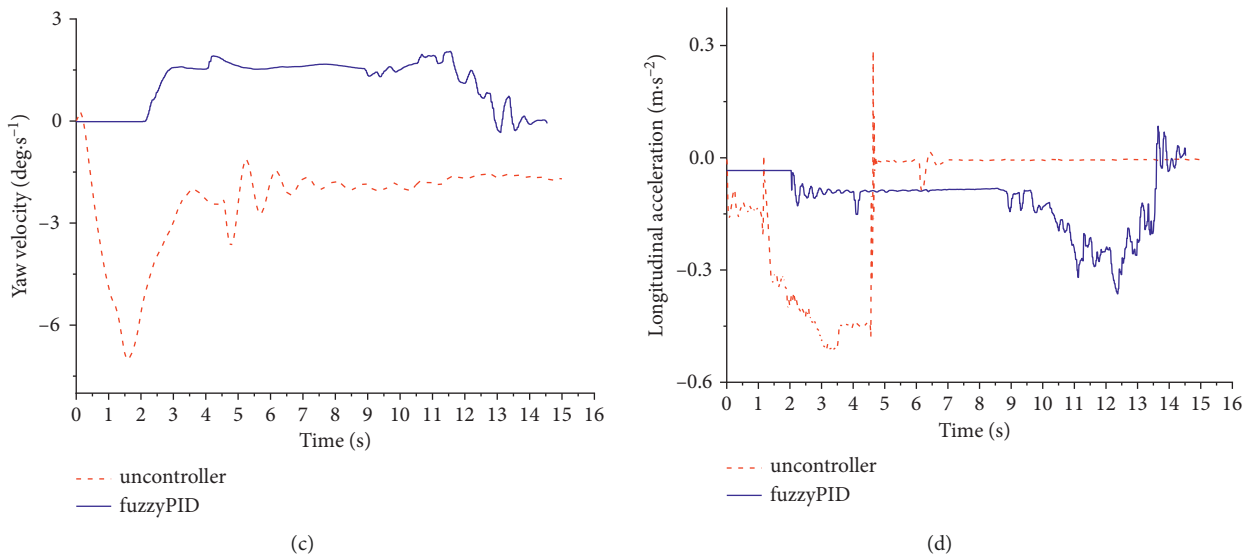

Figure 32: HIL test diagram under curve operating conditions when $u = 0.5$. (a) Braking distance. (b) Lateral acceleration. (c) Yaw velocity. (d) Longitudinal acceleration.

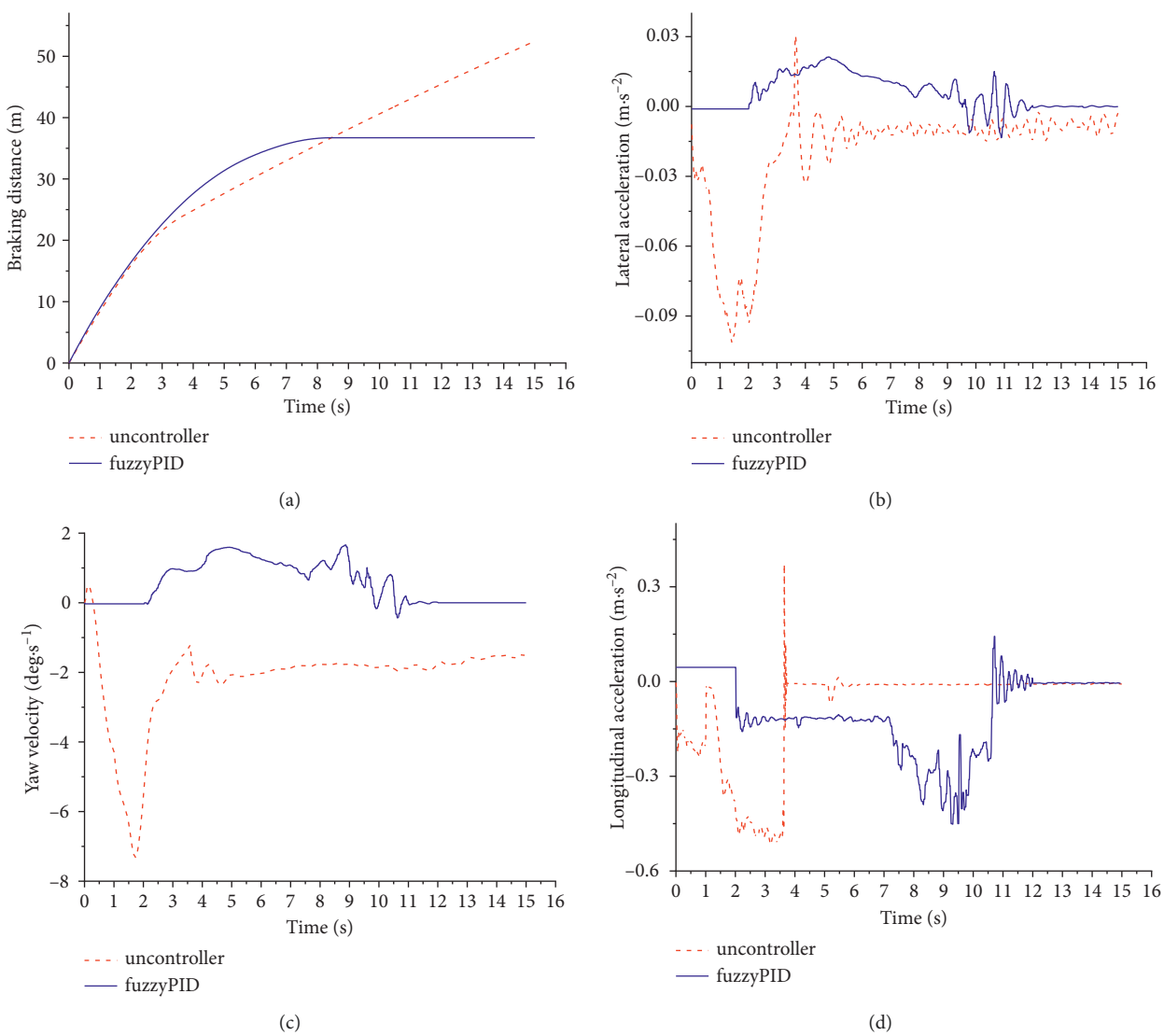

Figure 33: HIL test diagram under curve operating conditions when $u = 0.8$. (a) Braking distance. (b) Lateral acceleration. (c) Yaw velocity. (d) Longitudinal acceleration.

principle is carried out on the DFL1250A12 three-axis chassis real vehicle of Dongfeng series. The hardware platform consists of driving simulator, chassis brake bench, wheel speed simulator, electrical cabinet, and so on. The transmission of the upper computer and the lower computer is connected to the real vehicle through the electrical cabinet and wheel speed simulator. Finally, the three-axis chassis vehicle electronic control comprehensive experimental platform is started, and the physical diagram is shown in Figure 27.

The HIL experimental operation mainly establishes the connection between the upper computer and the lower computer and connects the Simulink model and the real vehicle chassis. Through the comparative analysis of the sliding film control and fuzzy PID control in the simulation, it is found that the designed fuzzy PID control strategy has better control effect on the active safety braking stability of vehicles. Therefore, only fuzzy PID is used for the HIL test.

4.2. HIL Verification under Downhill Condition. The hardware verification test continued to take the complete failure of the right front wheel of the vehicle as an example, driving on the downhill road with the road adhesion coefficient of 0.4, 0.5, and 0.8, respectively. In addition, it is due to the hysteresis factor of the hardware-in-the-loop test itself, the response time of the model is longer than that of TruckSim simulation, which will lead to the extension of braking distance and other factors, and the hardware verification data are shown in Figures 28–30.

According to the hardware test in the figure above, when $u = 0.4$, $u = 0.5$, and $u = 0.8$, the braking distance of the vehicle gradually decreases as the road adhesion coefficient increases. A high road adhesion coefficient has a great positive effect on the vehicle. Although the yaw of the vehicle increases during braking, it is smaller than that of the vehicle with low road adhesion coefficient. The HIL test of heavy vehicles on downhill road shows that the braking distance of vehicles can still be effectively shortened and the active safety of vehicles can be improved.

4.3. Analysis of HIL Verification under Curved Operating Conditions. To further verify the braking effect of the real vehicle and facilitate analysis, the HIL experiment is carried out according to the actual situation. At the same time, the hysteresis effect still exists in the curve test process, and the hardware verification data are shown in Figures 31–33.

The HIL test data under different road adhesion coefficients show that the model is still effective in controlling the right front wheel fault, but the braking distance is too large when the vehicle brakes without control mode. Under the action of fuzzy PID controller, the vehicle braking stability and handling stability are effectively improved.

5. Conclusion

Based on the complete braking failure of vehicles, this study introduces the Monte Carlo method and designs the interval uncertain braking control strategy model to analyze the incomplete braking failure of vehicle's single wheel. To achieve the braking performance of the vehicles more effectively, the single-wheel braking force distribution strategy and the vehicle braking force distribution strategy are designed. Two kinds of control strategies of fuzzy PID control and sliding mode control are designed. When the vehicle runs at a safe speed under special road conditions, the longitudinal and lateral stability generated during braking is improved to a certain extent. Through multi-body dynamic simulation, in multi-body dynamic simulation, although the improvement of fuzzy PID control in braking distance is not as good as that of sliding mode control, it is better than sliding mode control in yaw control, longitudinal control, and lateral control. Therefore, fuzzy PID control is used as the optimal controller combined with vehicle braking model for the HIL experiment. Due to the hysteresis effect of the HIL platform itself, the data results of the HIL platform have several seconds delay compared with the simulation analysis data, but compared with the uncontrolled model, the vehicle handling stability is greatly improved.

Data Availability

The braking control data of HIL used to support the findings of this study are included within the article.

Conflicts of Interest

The authors declare no conflicts of interest.

Acknowledgments

This work was supported by National Natural Science Foundation of China (grant nos. 12072204 and 11572207), Natural Science Foundation of Hebei Province (grant no. A2020210039), and Independent Subject of State Key Laboratory of Mechanical Behavior and System Safety of Traffic Engineering Structures (ZZ2020-32).

References

[1] Q. Xu and X. Bai, "Study on the cause of vehicle braking failure in road traffic accident [J]," *China Forensic Science*, no. 4, pp. 99–102, 2020.

[2] Y. Yang, Z. Yuan, J. Chen, and M. Guo, "Assessment of osculating value method based on entropy weight to transportation energy conservation and emission reduction[J]," *Environmental Engineering & Management Journal (EEMJ)*, vol. 16, no. 10, 2017.

[3] J. Gong, Y. Luo, Z. Qiu, and X. Wang, "Determination of key components in automobile braking systems based on ABC classification and FMECA[J]," *Journal of Traffic and Transportation Engineering*, vol. 9, no. 1, pp. 69–77, 2020.

[4] Q. He, "Analysis and countermeasures of heavy truck safety accident [J]," *Automotive Engineer*, no. 8, pp. 45–47, 2020.

[5] W. Wang, "Statistical analysis of road traffic safety accidents in China [J]," *China work safety*, vol. 15, no. 03, pp. 52-53, 2020.

[6] Z.-x. Wang, Q. Yu, F. Han, and P.-l. Shi, "Research on a brake temperature model of heavy-duty trucks braking on long

downhill," *Journal of Highway and Transportation Research and Development*, vol. 10, no. 3, pp. 90–96, 2016.

[7] D. Kim and H. Kim, "Vehicle stability control with regenerative braking and electronic brake force distribution for a four-wheel drive hybrid electric vehicle," *Proceedings of the Institution of Mechanical Engineers - Part D: Journal of Automobile Engineering*, vol. 220, no. 6, pp. 683–693, 2006.

[8] P. Spichartz, T. Bokker, and C. Sourkounis, "Comparison of electric vehicles with single drive and four wheel drive system concerning regenerative braking," in *Proceedings of the 2017 Twelfth International Conference on Ecological Vehicles and Renewable Energies (EVER)*, pp. 1–7, IEEE, Monte Carlo, Monaco, April 2017.

[9] J. Nah and S. Yim, "Vehicle stability control with four-wheel independent braking, drive and steering on in-wheel motor-driven electric vehicles," *Electronics*, vol. 9, no. 11, p. 1934, 2020.

[10] G. Moreno, L. C. Nicolazzi, R. D. S. Vieira, and D. Martins, "Suspension and tyres: stability of heavy vehicles," *International Journal of Heavy Vehicle Systems*, vol. 24, no. 4, p. 305, 2017.

[11] F. Yakub and Y. Mori, "Heavy vehicle stability and rollover prevention through switching model predictive control," in *Proceedings of the 2015 10th Asian Control Conference (ASCC)*, pp. 1–6, IEEE, Kota Kinabalu, Malaysia, June 2015.

[12] J. Yao, "Finite element analysis for commercial vehicle drum brakes,"vol. 5, pp. 1247–1251, in *Proceedings of the 2021 IEEE 5th Advanced Information Technology, Electronic and Automation Control Conference (IAEAC)*, vol. 5, IEEE, Chongqing, China, March 2021.

[13] H. Jiang, W. Zhou, C. Liu, G. Zhang, and M. Hu, "Safe and ecological speed control for heavy-duty vehicles on long-steep downhill and sharp-curved roads," *Sustainability*, vol. 12, no. 17, p. 6813, 2020.

[14] S. Rajendran, S. K. Spurgeon, G. Tsampardoukas, and R. Hampson, "Estimation of road frictional force and wheel slip for effective antilock braking system (ABS) control," *International Journal of Robust and Nonlinear Control*, vol. 29, no. 3, pp. 736–765, 2019.

[15] W. Li, X. Zhu, and J. Ju, "Hierarchical braking torque control of in-wheel-motor-driven electric vehicles over CAN," *IEEE Access*, vol. 6, pp. 65189–65198, 2018.

[16] H. Zheng, S. Ma, and Y. Liu, "Vehicle braking force distribution with electronic pneumatic braking and hierarchical structure for commercial vehicle," *Proceedings of the Institution of Mechanical Engineers - Part I: Journal of Systems & Control Engineering*, vol. 232, no. 4, pp. 481–493, 2018.

[17] B. Xia, H. Lü, D. Yu, and C. Jiang, "Reliability-based design optimization of structural systems under hybrid probabilistic and interval model," *Computers & Structures*, vol. 160, pp. 126–134, 2015.

[18] M. R. Wang, J. P. Fan, and J. Hu, "A non-probabilistic reliability-based design optimization method for structures based on interval models," *Fatigue and Fracture of Engineering Materials and Structures*, vol. 41, no. 2, pp. 425–439, 2018.

[19] Y. Yang, K. He, Y. p Wang, Z.-z. Yuan, Y.-h. Yin, and M.-z. Guo, "Identification of dynamic traffic crash risk for cross-area freeways based on statistical and machine learning methods," *Physica A: Statistical Mechanics and Its Applications*, vol. 595, Article ID 127083, 2022.

[20] H. Lü and D. Yu, "Brake squeal reduction of vehicle disc brake system with interval parameters by uncertain optimization," *Journal of Sound and Vibration*, vol. 333, no. 26, pp. 7313–7325, 2014.

[21] Z. Kang, Y. Luo, and A. Li, "On non-probabilistic reliability-based design optimization of structures with uncertain-but-bounded parameters," *Structural Safety*, vol. 33, no. 3, pp. 196–205, 2011.

[22] H. m Li, X. b Wang, S. b Song, and H. Li, "Vehicle control strategies analysis based on PID and fuzzy logic control," *Procedia Engineering*, vol. 137, pp. 234–243, 2016.

[23] C. Li, C. He, Y. Yuan, and J. Zhang, "Co-simulation on performance evaluation of a new electronic control hydraulic braking system," in *Proceedings of the 2018 IEEE 3rd Advanced Information Technology, Electronic and Automation Control Conference (IAEAC)*, pp. 2500–2504, IEEE, Chongqing, China, October 2018.

[24] Z. P. Sun, W. H. Kang, G. C. Wan, and M. S. Tong, "A fuzzy PID controller with neural network algorithm for freight trains' braking system," in *Proceedings of the 2019 Photonics & Electromagnetics Research Symposium-Fall (PIERS-Fall)*, pp. 2646–2651, IEEE, Xiamen, China, December 2019.

[25] L. He, W. Ye, Z. He, K. Song, and Q. Shi, "A combining sliding mode control approach for electric motor anti-lock braking system of battery electric vehicle," *Control Engineering Practice*, vol. 102, p. 104520, Article ID 104520, 2020.

[26] X. Ma, P. K. Wong, J. Zhao, and Z. Xie, "Cornering stability control for vehicles with active front steering system using T-S fuzzy based sliding mode control strategy," *Mechanical Systems and Signal Processing*, vol. 125, pp. 347–364, 2019.

[27] X. Ji, X. He, C. Lv, Y. Liu, and J. Wu, "A vehicle stability control strategy with adaptive neural network sliding mode theory based on system uncertainty approximation," *Vehicle System Dynamics*, vol. 56, no. 6, pp. 923–946, 2018.

[28] B. Li, S. Chang, X. Zhu, and M. Yang, "Research on braking in a turn and parameter optimization of centre-axle trailer combination based on TruckSim," *Journal of Physics: Conference Series*, vol. 1986, no. 1, p. 012138, Article ID 012138, 2021.

[29] M. K. Salaani, D. Mikesell, C. Boday, and D. Elsasser, "Heavy vehicle hardware-in-the-loop automatic emergency braking simulation with experimental validation[J]," *SAE International Journal of Commercial Vehicles*, vol. 9, no. 2, pp. 57–63, 2016.

[30] L. Li, T. Guo, and S. Xu, "Simulation analysis of vehicle handling stability based on Trucksim[C]//Journal of physics: conference series," *Journal of Physics: Conference Series*, vol. 1885, no. 3, Article ID 032043, 2021.

[31] R. M. Ashby, "Hardware in the loop simulation of a heavy truck braking system and vehicle control system design," *The Ohio State University*, 2013.

[32] Y. Chen, S. Chen, T. Zhang, S. Zhang, and N. Zheng, "Autonomous vehicle testing and validation platform: integrated simulation system with hardware in the loop," *2018 IEEE Intelligent Vehicles Symposium (IV)*, pp. 949–956, IEEE, 2018.

[33] O. U. Acar, L. Güvenç, and E. Altuğ, "Hardware-in-the-Loop testing of automatic lift dropping system for heavy trucks," *Journal of Intelligent and Robotic Systems*, vol. 98, no. 3-4, pp. 693–703, 2020.